Virtual Source Modelling of Photon Beams for Monte Carlo Based Radiation Therapy Treatment Planning

Marcin Paweł Sikora

Dissertation for the degree doctor philosophiae (dr.philos.)
at the University of Bergen

Dissertation date: 13.10.2011

This thesis is dedicated to my mother
who gave me a strength to finish this work.

Scientific environment

This study was carried out at the Department of Biomedical Physics, University Hospital in Tübingen, Germany. During period 2003-2004 in the frame of the Marie Curie fellowship invited by Prof. Fridtjof Nüsslin under supervision of Dr. Matthias Fippel and during 2004-2009, with Dr. Markus Alber as principal adviser. Further, there was scientific collaboration during parts of the study with Elekta Monte Carlo research group, Crawley, UK and CMS Software group, St. Luis, USA which is now part of Elekta group. The study included a 6 month working period in 2010 at the Department of Boiomedicine of University of Bergen with cooperation with Prof. Arvid Lundervold and finally at Section of Medical Physics in Haukeland University Hospital in Bergen with the head of Section of Medical Physics, Anfinn Mehus.

Acknowledgements

The main part of the work presented in this thesis was carried out in Germany when working at the Biomedical Physics group in Tübingen and the final steps in completing it were done in Norway at the Biomedicine research group of University of Bergen and the Department of Oncology and Medical Physics, Haukeland University Hospital. During all years of this work I have met a number of people to whom I am deeply obliged.

First and foremost, I thank my supervisor Dr. Markus Alber. His enormous working capacity, broad knowledge, methodological talents, incredible ability to explain problems in the most picturesque way were invaluable sources of my inspirations for this work. Also his scientific intuition and wise advises were key factors for the work presented here. I thank him also for the great times we enjoyed together after work during tango milongas and during our unforgettable hiking trips.

Thanks to formal and present members of the Biomedical Physics group in Tübingen with whom I have enjoyed my time in Germany. I acknowledge the debt I owe to Matthias Fippel who introduced me into the MC world by showing his concepts of virtual head modeling. Special thanks I own to my best friend and office-mate Matthias Söhn as well as to his wife Mary Kim. Together we spent unforgettable time in the office and privately after work next to a cup of coffee, wine or beer, sharing our good and bad experiences. Similarly, to Niklas Rehfeld for his great sense of humor which made my days joyful. Jan Muzik for his input to my work with his film measurements but also for his calm attitude and friendship. Martin Soukup for sharing his knowledge about MC and possibilities to discuss my work with him. Oliver Dohm for sharing his experience and advises in dosimetric measurements. Urszula Jeleń for being a good friend over many years. Thanks to Daniela Thorwarth, Benjamin Sobotta, Chrostoph Baum, Sabine Pinstaske and others who contributed to the excellent working atmosphere in Tübingen.

I thank also members of the MC Elekta group for cooperation in implementing my model in MC treatment planing system Monaco, especially; Jose Luis Dumond, Mary Napolitano, Sergey Golubev, Oleg Krivosheev and Gustav Meedt.

I am also thankful to my colleagues in Norway. People from the Boiomedicine group of University of Bergen; especially Prof. Arvid Lundervold and Are Losnegård for sharing their experience in medical imaging and being good fellows and companions during my half year MedViz project as well as my new colleagues at Section of Medical Physics in Haukeland University Hospital in Bergen. Especially the head of Section of Medical Physics, Anfinn Mehus. His long time experience in radiotherapy and skills in coordinating work-flow have created a great opportunity for me in learning practical as a medical physicist things but also for leaving a possibility for developing research activities. And last but not least, to the head physicist in the PET center in Haukeland Universyty Hospital, Odd Harald Odland, who made remarkable effort in finalising my thesis by his precise comments and by coordinating my deface of it together with Prof. Arvid Lundervold.

With gratefulness I would like to thank also my family. Especially to my mother to whom

I dedicate my thesis. Although, she is not longer between us, I am sure she would be very proud of her little Marcinek. My parents made it possible for me to promote in my education and develop my knowledge as well as my hobbies.

Thanks to this thesis it happen the most wonderful thing in my life. I have met my friend, tango partner and wife - Liv Bolstad Hysing. She was invaluable assistance during finishing this manuscript and she is my infinitive source of energy and motivation in everyday life. Without her together with our son, Emil, I would not go so far.

Abstract

Modern radiotherapy (RT) techniques such as stereotactic body radiotherapy (SBRT), intensity-modulated radiotherapy (IMRT) or volumetric modulated arc therapy (VMAT) carries the potential of improving the quality of treatment. However, they often lead to complex beam arrangements where the effects of electron transport can only be handled by Monte Carlo (MC) dose calculation algorithms. The biggest obstacle for use of MC in RT is an accurate and efficient beam model which is able to model clinical beams with all the imports of a broad radiation field which is specific to each treatment machine. We have applied the concept of virtual source modelling to develop such a beam model based on the following ideas:

- identification of the nature of beam components by a full MC simulation of the accelerator head,
- identification of models and reference parameters which are universal,
- definition of a few open parameters that need to be tuned by reliable measurements,
- development of a robust commissioning method by poly-energetic kernels,
- performing simultaneous validation of the beam model during commissioning.

The resulting Virtual Source Model (VSM) employs three sources representing three distinguishable beam components: primary photons, secondary photons and electron contamination. Each source is described by analytical functions with two types of parameters (1) *reference parameters* fixed based on the full MC data analysis and (2) *open parameters* which are fitted during commissioning of the model for each individual accelerator. The sources reproduce a variety of effects which are present in broad clinical beams by employing the following corrections:

- off-axis energy softening for primary and secondary photons,
- absorption/scatter in the flattening filter,
- energy fluence normalisation,
- energy fluence flatness and particle fluence central depression for primary photons,
- correction for energy-focussing of the source distribution for secondary photons and contamination electrons,
- enhancement of the focus spot particle fluence for contamination electrons.

The developed model was commissioned and validated for clinical use for 6 MV and 15 MV beams of two types of Elekta linacs equipped with a standard leaf-width MLC (leaf width 1 cm@isocentrum) and a mini-MLC (leaf width 4 mm@isocentrum). Several tests were performed for various beam arrangements. The MC dose calculation with the VSM shows excellent agreement with measurements in water and in a heterogeneous lung phantom, both for rectangular fields from 0.8x0.8 cm^2 to 40x40 cm^2 as well as for complex IMRT fields. For complex IMRT beams measured in water, the agreement was within 3%/2 mm inside the field and 5%/2 mm outside the field (tails of cross profiles) for 6 MV and 15 MV beam, respectively. While 3%/3 mm agreement was achieved between MC calculated dose and film measurements in the lung phantom.

In conclusion, a VSM for a clinical broad photon beam was developed which is accurate and efficient. The VSM model overcomes problems related to full MC simulation of the accelerator head like long simulation time, cumbersome commissioning routine and dependency on the technical information about the accelerator head. This VSM enables a broad implementation of MC-TPS in clinical routine.

List of papers and presentations

The main ideas of this thesis were published in following papers[1]:

1. M. Sikora, O. Dohm and M. Alber: *A virtual photon source model of an Elekta linear accelerator with integrated mini MLC for Monte Carlo based IMRT dose calculation*. Phys Med Biol 52(15), volume 52, 4449–63, August 2007

2. M. Sikora and M. Alber: *A virtual source model of electron contamination of a therapeutic photon beam*. Phys Med Biol 54(24), volume 54, 7329–44, December 2009

3. M. Sikora, J. Muzik, M. Söhn, M. Weinmann and M. Alber: *Monte Carlo vs. pencil beam based optimization of stereotactic lung IMRT*. Radiat Oncol 4, volume 4, 64, 2009

Ideas and results have been presented at the following conferences and workshops:

1. M. Sikora: *Monte Carlo beam modeling for photon therapy treatment planning*. II metodo Monte Carlo in Radioterapia, practica clinica e strumenti tecnologici, 30-31 October 2006, Catania, Italy

2. M. Sikora and M. Alber*: Application of a photon Virtual Source Model of a mini-MLC for MC dose calculation of small IMRT fields.* 1st European Workshop on Monte Carlo Treatment Planning of the European Workgroup on MCTP, 22-25 October 2006 Gent, Belgium

3. M. Sikora, O. Dohm, Z. Tung and M. Alber: WE-C-AUD-09: *Dose Accuracy Gains by Use of Monte Carlo in Routine IMRT Treatment Optimization.* Medical Physics 34(6), volume 34, AAPM, 2591–2591, 2007

4. M. Sikora: *Monte-Carlo or patient specific QA?* ESTRO course on IMRT and Other Conformal Techniques, Tübingen, Germany , May 2008

5. K.M. Niyazi, O. Dohm, Z. Tung, M. Sikora and M. Alber: Monte Carlo simulation of a multi-wire ionisation chamber for real-time verification of dynamic IMRT delivery, the 27^{th} ESTRO meeting in Göterborg, Sweden, 2008

6. M. Sikora: Implementation and use of Monte Carlo methods in the clinic. Winterschule für Medizinische Physik, 23-25 March 2011, Pichl, Austria

[1] Reprints were made with permission from publishers

Contents

Nomenclature

3D	three-dimensional
BM	Beam Modulator
CP	cross profile
CT	computer tomography
DDC	depth dose curve
eVSM	virtual source model of the electron contamination
IMRT	intensity-modulated radiotherapy
linac	linear accelerator
MC	Monte Carlo
MC-TPS	Monte Carlo based Treatment Planning System
MLC	multi-leaf collimator
OF	output factor
PS	Phase Space
RT	radiotherapy
SBRT	stereotactic body radiotherapy
SC	secondary collimator
SP	scoring plane
SSD	Source Surface Distance
T&G	Tong&Groove
VMAT	volumetric modulated arc therapy
VSM	Virtual Source Model

Chapter 1

Introduction to Monte Carlo Simulations

1.1 Fundamentals of Monte Carlo Simulations

The main goal of this work is to present a model that will contribute in enabling clinical use of Monte Carlo based models of medical linear accelerators and Monte Carlo calculated dose distributions for Radiation Therapy dose planning.

A Monte Carlo (MC) Simulation is a statistical method of finding a solution for an integral equation by a repetition of random sampling of possible outcomes of different interaction processes which are calculated from probability distributions representing the different possible physical processes and interactions. The Monte Carlo method is especially useful when there is no analytical solution to a problem or an integral problem has a large number of dimensions. It is a powerful method for modelling and calculation of particle and radiation transport through complex geometries. In the context of particle transport processes, it is possible to imagine a simulation step as holding the fate of a single particle making its way through a predefined geometry setup. This is enabled through precalculated probabilities for which interactions that such a particle will possibly undergo in that step. A single particle trajectory is often referred to as particle history. The accuracy of a simulation result depends on the number of simulated histories, as the number of histories effectively represents the level of the statistics, i.e. a high number of histories will enable an emulation of the statistical nature of the fundamental interaction processes involved.

In Radiation Therapy (RT), like in other contexts where one is applying Monte Carlo calculations, Monte Carlo dose calculations are used to simulate individual tracks of photons and electrons. When calculation radiation transport through a medical linear accelerator, the particle tracking is starting at the bremsstrahlung producing target, continuing through the collimators in the accelerator head and continues further into the patient. Along its track, a particle interacts with matter in various processes: coherent and incoherent scattering, absorption and pair production, depending on the interaction cross sections and the particle's energy.

In all instances of interaction it is common to store information about:

- the position where the interaction takes place,
- the amount of deposited energy,
- the distance to the next interaction,
- the direction of the involved particle(s),

- the probability of creation of secondary particles or a probability of absorption of the particle.

As these entities are calculated and stored, the chain of calculation goes on until the simulated particle drops below a pre-set cut-off energy. By adding the contribution from all interactions of a large number of histories, for instance the absorbed energy is calculated.

1.2 Rationale for a Monte Carlo Treatment Planning System

The origin of 3-dimensional (3D) RT planning can be connected to the invention of computer tomography (CT) in 1971 by Godfrey Hounsfield. This allowed for a much more accurate determination of the target volume(s) using tomographic images of the patient anatomy and it also forms the basis for an accurate 3D dose computation. Conventional dose calculation algorithms (Pencil Beam, Superposition/Collapsed Cone) are based on analytical models of radiation transport and their use requires extensive sets of measurements in order to verify the validity of the algorithms. These algorithms are very successful due to their speed and accuracy in conventional RT. They struggle, however, to meet the accuracy criteria when challenged by modern radiotherapy techniques like stereotactic body radiotherapy (SBRT), intensity-modulated radiotherapy (IMRT) or volumetric modulated arc therapy (VMAT), where the Treatment Planning System (TPS) has to handle quite complex beam arrangements, usually composed of very small fields where the lack of electron equilibrium is present. In such situations the explicit simulation of secondary electrons is relevant to achieve the accurate dose distribution calculation [12]. Moreover, the high efficiency of conventional algorithms drops rapidly with the number of calculated beams. Therefore they also become less suited for rotational radiotherapy treatment planning with its continuous irradiation of the patient while the linac gantry head is in motion.

The Monte Carlo MC method has been shown through many research studies to calculate accurate dose distributions for clinical radiotherapy [12]. A required accuracy of 2%-3%, for the dose calculation, regardless of beam geometry, beam arrangement and patient composition [24], can be provided by Monte Carlo simulations [77, 12]. In highly modulated beams, often composed of small and complex shaped segments [70, 48, 55, 3, 71, 4, 50, 73, 16, 17, 10, 36], Monte Carlo dose computation is recommended for use in the presence of lateral electron disequilibrium [24]. MC algorithms simulates secondary electrons explicitly, they are expected to be capable of more accuracy than other kinds of calculation algorithms [24]. Therefore, Monte Carlo is the mose accurate dose calculation algorithm for use in radiotherapy. The accurate dose calculation is an important part os the treatment planning process which has a direct inpact on the quality of the treatment [77].

The biggest obstacle for use of a Monte Carlo algorithm in radiotherapy is that it has to model clinical beams with all the imports of a broad radiation field which is specific for each linear accelerator treatment machine. It has been a conventional assumption in the past, that MC simulation are too time consuming for clinical use [75]. However, the increased computation power of modern computers in combination with an efficient beam model and variance reduction techniques make it feasible to bring all advantages of the MC method to the clinical routine and improve the quality of treatment planning.

1.3 Modularity of a Monte Carlo System

An important feature of Monte Carlo simulations is the built in modularity of the method. It is possible to subdivide the simulations into different independent parts. Thus; each step of the simulation and particle tracking, from when the beam of electrons are impinging on the bremsstrahlung producing target, to the step where the dose calculation in the patient is performed, can be performed separately. In the context of modelling and simulations of dose production from a medical linear accelerator; at the highest level, the Monte Carlo simulations can be divided into two parts:

1. *An accelerator head part* - a simulation of the particle production and collimation which can be represented by a detailed or parameterized head model.

2. *A patient part* - a simulation of the radiation transport through the patient geometry.

There are several good reasons for splitting MC simulations into different independent (sub) parts. The material composition on the very detailed level of an individual accelerator head, is in general uncertain or unknown in advance. A detailed description of the accelerator head geometry is cumbersome to obtain. The geometry of the accelerator head changes only at the lower part which is responsible for beam modulation. Therefore, the invariant part of the accelerator head is simulated only once (this is after the model of the invariant part is developed and ready) and, the results of the simulations can be represented by key particle information stored in so-called Phase Space (PS) files or parametrized in a process referred to as an accelerator head modelling process.

1.4 Production of External Photon Beams for Radiation Therapy

Photon beams are the almost exclusively applied source for external beam radiation in modern Radiation Therapy. Typical components of the accelerator head are presented in Figure 1.1. The therapeutic photon beams are also called broad photon beams since they can cover large areas of up to 40x40 cm^2 large photon fields at the so-called isocenter plane. The photon beams are produced in compact medical linear accelerators (linacs) by bombarding an electron pencil beam, accelerated up in energy in a waveguide tube, onto a high-Z metal target and thereby effectively converting the electron's energy into bremsstrahlung photons that constitutes the (unmodulated) photon beam. The bremsstrahlung radiation which is emitted in a wide cone is collimated by a primary collimator. Then, it is modulated by a flattening filter in order to produce a flat energy distribution of the beam. Two additional elements are a monitor chamber and a field mirror. The monitor chamber registers the amount of radiation generated by the linac. The mirror projects a light field of the beam setup onto the surface of the patient. The beam shape is formed according to the doseplan requirements for each individual patient by secondary collimators which are also referred to as beam modifiers. They typically comprise solid jaws movable in the inplane (y) and crossplane (x) directions and a multi-leaf collimator (MLC) positioned below these for further fine-tuning of the beam shape. The MLC contains 40-80 pairs of leaves which can conform to complex shapes while jaws reduce the radiation passing through and between the MLC leaves within a rectangular outline (Figure 1.1). The jaws are thick metal blocks which reduce, when it is possible, the radiation collimated by the MLC.

The accelerator head can be divided into two main parts:

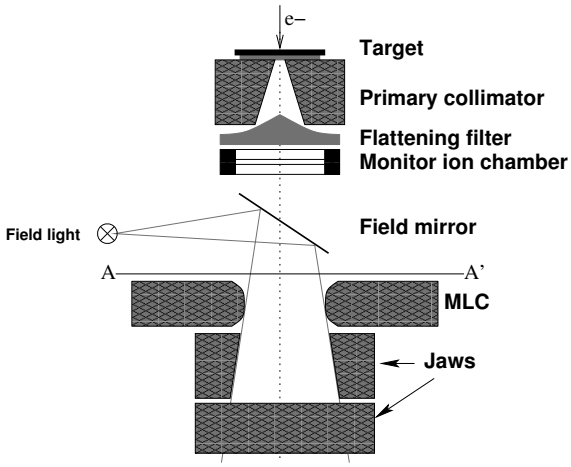

Figure 1.1: Schematic drawing of the typical elements of an accelerator head. The A-A' plane separates the upper (patient invariant) part of the linear accelerator head from the lower (patient dependent) part of the linear accelerator head.

1. the invariant part (target, primary collimator, flattening filter, monitor ion chamber, field mirror),

2. the patient dependent part (MLC and collimator jaws).

The invariant part of the accelerator characterises the radiation source while the patient dependent part derives from the patient specific treatment plan.

1.5 Beam Modelling approaches

The detailed modelling of the linear accelerator head is the natural starting point of the Monte Carlo based Treatment Planning System (MC-TPS). In figure 1.1, a schematic drawing of a standard linear accelerator head can be seen. The accuracy of the dose calculation in a practical setting depends crucially on a precise enough description of the geometry and composition of the head of the linear accelerator. The second part of the process with calculation of the dose distribution in the patient uses well benchmarked MC dose engines which are general purpose MC codes [53, 31, 6, 19, 25, 9, 60] or codes dedicated for radiotherapy [47, 79, 62, 61, 32, 20]. The dedicated algorithms are more suitable for radiotherapy, since they are optimized for the therapeutic energies $\leq$ 25-50 MeV and with the particle composition of biological materials ranging from lung tissue to bony structures. These algorithms can be verified to very high accuracy in idealized experimental setups without problematic properties of the beam of a clinical accelerator.

In order to be able to perform Monte Carlo based studies of the output from a linear accelerator; a considerable amount of work has to be spent on the so-called beam modelling. The aim of beam modelling is to describe the individual properties of a beam produced by a particular medical linear accelerator. In order to avoid time (and cpu) consuming calculations of the trajectories of a high number of particles' stepwise trajectories through the whole linear accelerator head each time a Monte Carlo based doseplan is made, efficiency steps has to be

taken. Thus, alternative methods have been devised in order to avoid a simulation of the invariant part of the accelerator head for each individual Monte Carlo computation of dose to the patient. This is possible due to the described modularity of a normal MC simulation setup. The separate simulation of the invariant part of the accelerator will, optimally, be performed only once and from then on being represented by a beam model. Based upon this, the beam model is used to reconstruct particle properties, i.e. energy, direction, origin location, statistical weight, etc., referred to as the Phase Space information, or simply the Phase Space (PS), for further MC transport through the patient dependent part of the accelerator head and into the patient.

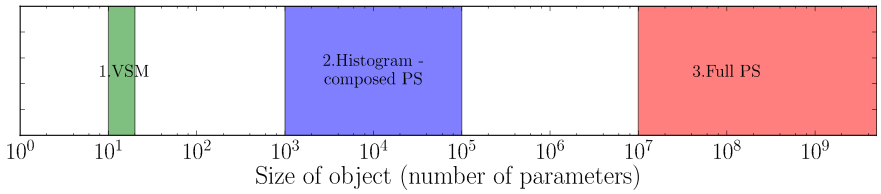

Figure 1.2: The number of parameters used to define three types of beam models: (1) Virtual Source Model (VSM), (2) Histogram - compressed PS and (3) Full PS.

1.6 Phase Space Information: Storage of Particle Properties

There are three main approaches of beam modelling ordered by the degree of compression of the Phase Space information (Figure 1.2).

1.6.1 Phase Space file

Monte Carlo systems use a geometrical model to perform the MC simulation of a large number of histories ($10^8 - 10^9$) of particle transport [59, 25]. The transport begins where the primary electron beam is streaming out the exit window of the acceleration tube (just in front of the target) to a so-called scoring plane (SP) located at chosen positions in the accelerator head. When a particle crosses a scoring plane, its properties are recorded in a Phase Space (PS) file and a PS based dataset for secondary particles is created during the particle simulation.

Since a substantial fraction of the simulated histories end before reaching the SP due to absorption and/or scatter processes, the full stepvise MC simulation of the accelerator head is not necessarily the best approach. The whole process with step by step simulating and re-simulating all the processes that takes place, each time a doseplan is made, has some clear disadvantages with respect to the time needed in order to calculate the doseplan. In order to reduce the total simulation time, the result of a full Monte Carlo simulation is recorded in PS files, containing particle and particle property information recorded in the plane or in multiple planes in question, at the exit of the invariant part of the accelerator. These files are reused later as a particle generator for MC simulation of the patient specific, lower, part of the accelerator.

The main advantage of storing Phase Space information from certain scoring planes is thus that this information can be used, over and over again, as reference data since it is easy accessible and represents the results of the full MC simulation of the accelerator head in a quite condensed format.

The commissioning process of the full MC beam model is cumbersome because the properties of the primary electron beam have to be set empirically in a trial and error process, since their direct measurement is normally not possible in the clinical environment. On the other hand, the PS files contain a large amount of particles which can not pass the secondary collimation system due to absorption and scatter processes, this makes the PS files somewhat inefficient as particle generators for the calculations that is based upon this information. An efficiency test based on full MC simulations for the purpose of this work, showed that around 60% of the particles leaving the invariant part of the accelerator head will reach the patient, this even for the largest field size 40x40 cm^2. Since the information from PS files are time consuming and cumbersome to obtain and validate, they are in general unsuited as particle generators for Monte Carlo based treatment planning systems which has a built in requirement of rapid dose calculation for each individual doseplan.

1.6.2 Histogram Storage of Phase Space Information

A concept of PS parametrization in the form of histograms was introduced by the PEREGRINE group[61]. This group performed a detailed study on the influence of linac components on the photon fluence, on the energy spectra and on the angular distributions of the photons while using the BEAM [59] and MCNP [9] codes to model a series of Varian linacs. Their proposed algorithm increased the efficiency of particle generation to 96% compared to the efficiency of particle generation from the Phase Space file for the largest field size 40x40 cm2. Also, it reduced the size of the PS file from several gigabytes to a few kilobytes of parameters describing fluence, angular and energy distributions of photons originating in the target, the primary collimator and the flattening filter (Figure 1.2). A similar concept was used by[23] which incorporates an algorithm modifying PS histograms of twelve sources (including jaws) in the linac head depending on the field size. Although the histogram based model improves the efficiency of particle generation as compared to the full simulation it is still complex due to its large number of parameters (Figure 1.2). For example, in order to generate one particle from the electron target, it is required 14 random numbers and further required values from typically 3 to 4 Look-Up tables[61].

1.6.3 Virtual Source Parametrization

The basic idea of virtual source modelling is to parametrize the PS results with a set of virtual sources which represent main beam components like primary photons, head scatter or electron contamination. Sources are defined by parameters derived from full MC simulations [46, 45, 41, 79, 39, 14] or measurements [21]. PS are compressed to a few parameters describing virtual sources whose properties are defined by analytical functions. The parameters of the beam model are derived from a commissioning routine which can be based on dosimetric measurements, results of full MC simulations or both together. The main advantages of virtual source modelling are that it is the most efficient particle generator and its accuracy can meet high clinical demands. Also, the commissioning routine is simple and robust as it fits a few open parameters to the set of measured commissioning data. The robust and easy commissioning helps to implement a MC-TPS in the clinical routine, since every linear accelerator has to be commission individually.

1.7 The Monte Carlo based Treatment Planning System Hyperion

The MC based TPS HYPERION [37, 1] has been used in clinical routine since 2002, when the first MC optimized and calculated IMRT treatment plan world-wide was delivered in Tübingen (Germany). At this time, a virtual photon energy fluence model, developed by [20] had been implemented. This model was then only validated for fields larger than 3x3 cm^2. The virtual photon energy model is quite unique, since it does not require a full MC simulation for its commissioning routine, but rather it is derived from dosimetric measurements in air and in water. A disadvantage of this approach is that the beam model accuracy depends on the measurement accuracy. Further, it has proved difficult to extract some of the model parameters robustly from the data. Especially measurements in air have substantial systematic errors due to different ion chamber response both to electrons (frequently reffered to as contamination electrons, due to the fact that the electrons are a bi-product from interactions within a photon beam) and photons and the compulsory use of a build-up-cup of a high-Z-material surrounding the detector. This may very well result in an inaccurate representation of the PS, which in turn leads to errors in dose calculations. New techniques like stereotactic radiosurgery or mini-MLC-based IMRT require high accuracy of the beam model, especially for very small fields, i.e. smaller than 3x3 cm^2. Therefore, improvements of the head model were necessary. This in turn, lead to the development of the Virtual Source Model presented in this work, preferably with an easier, less measurement dependent and less laborsome commissioning routine.

1.7.1 The Dose Engine in a Monte Carlo based Treatment Planning System

When photons and electrons enter the patient, the interactions that are taking place between the incoming particles and matter will produce the dose distribution applied for the Radiation Treatment purpose. The dose distribution is calculated by a dose engine which uses a virtual phantom representing an individual patient geometry. The virtual phantom is based on a Computer Tomography 3D distribution map of the Hounsfield Units translated into the 3D density map which is used by the dose engine for the dose calculation. There are two essentially different techniques for dose calculation used by the MC dose engines:

1. the KERMA approximation, and

2. Summation of deposited energy.

Using the KERMA, approximation one can discard secondary electron transport. This significantly speeds up the dose calculation. It is then assumed that the secondary electron equilibrium i.e. the amount of energy carried out of that volume by electrons, is equal to the amount of energy carried into it by electrons. Due to this assumption, this technique is often not accurate enough, but in some cases it may be applied to parts of the dose calculation (see below).

Summing the deposited energy does not use any approximations for the secondary electron transport. In this case,one needs to know for each particle, how much energy that entered in a voxel (a small calculation volume), and how much energy that left the voxel in question: the difference being the energy depositde in that voxel. Two Monte Carlo Codes were used in this work in order to calculate the dose in CT based patent phantoms: DOSXYZnrc [78] and XVMC [20]. The DOSXYZnrc code is a part of the BEAMnrc software which uses the EGSnrc [59] dose engine on any arbitrary voxel distribution with dimensions and material composition defined by user for each voxel or a 3D virtual phantom based on a CT scan. In both cases, the geometry and material composition has to be predefined before the calculations.

Although, the DOSXYZnrc code is applicable for actual Monte Carlo treatment planning calculations, large calculation times are the remaining drawback. The XVMC is a Monte Carlo code which is optimized for use in Radiotherapy. The stopping and scattering powers for the multiple-scattering simulation of electrons are determined directly from the Hounsfield number distribution and it needs no material specification. It was developed by Kawrakow et al (1996) [34] as a dose engine for electron beams (VMC) and extended for photons beam in the fast X-Ray Voxel Monte Carlo system (XVMC) by Fippel (1999)[20] and it was further optimized by Kawrakow and Fippel (2000) [33]. Then, the XVMC was coded in C++ by Kawrakow leading to the VCM++ [32] code . The high efficiency of the XVMC code is achieved by implementing several variance reduction techniques, such as photon splitting, electron history repetition, Russian Roulette, and the use of quasi-random numbers. An overview of these techniques can be found in [33]. It is also possible to further improve the efficiency by optimizing the transport parameters such as electron energy cut-off, maximum electron energy step size, photon energy cut-off and a cut-off for the KERMA approximation, without loss of calculation accuracy. The KERMA approximation (no explicit simulation of electron transport) is applied only to secondary or higher order photons with energy below the kerma cut-off [33]. Otherwise summing of the energy deposition technique is employed to calculate the dose. These methods makes the XVMC code 50-80 times more efficient compared to the EGS4/PRESTA dose engine and the dose calculation accuracy is on a sub-percent level when compared to EGSnrc for simulations in the energy and material range of interest for radiation therapy [33]. Due to the achieved high accuracy and efficiency, the XVMC dose engine in implemented in several MC based treatment planning systems which are already available on the market (BrainLab/XVMC , Elekta-CMS/XVMC, Hyperion/XVMC, Nucletron/VMC++).

Chapter 2

Modelling of the Head of a Clinical Linear Accelerator

2.1 General considerations

In this chapter, a Virtual Source Model (VSM or VS Model) approach for beam modelling is presented. The VS Model is derived from full scale simulations of the accelerator head with the BEAMnrc MC code system [59]. An efficient method of adjusting the socalled open parameters of the VSM is based on standard dosimetric measurements in water for each individual linear accelerator. The results obtained with the VSM show its degree of accuracy when compared to validation measurements. This accuracy is quite high as we will see in the following. The VSM, it turns out, provides an efficient and accurate particle generator for MC treatment planning systems used for Radiation Therapy. In a clinical context, MC simulations always start with the generation of particles by the use of a specific beam model of the linear accelerator. The MC generated particles are to be used as input for the necessary dose calculations in the patient performed with another MC dose engine. Because existing MC dose engines themselves are well benchmarked and validated, one has quite good knowledge about the level of accuracy in that part of the simulation process. The accuracy of the dose calculation in a patient is further also dependent on the accuracy of the beam model.

In order to perform an accurate full MC simulation of a linac beam, the following information is required:

- An accurate description of the primary electron beam impinging on the bremsstrahlung producing target [64].

- An accurate description of all parts of the linac head, including the geometrical layout, relative positions of the modules constituting the linac head and the material composition and density of the applied alloys and materials [2, 74]. It is important, but sometimes quite difficult, to obtain accurate information about each individual treatment machine from the linac manufacturer in this respect.

Further:

- The objective of the simulation, which itself can have influence on the results of the simulations by setting parameters such as cut-off energies or using variance reduction techniques [77], must be defined.

- The post calculation operation, i.e. reducing calculation uncertainties due to an insufficient number of simulated histories, which can lead to dose distribution degradation [51] or optimization convergence problems [22], must also be incorporated.

The described modularity of the MC simulation of clinical linear accelerators allows for dividing such a process into two main parts: (1) *the patient independent* (upper) part which remains fixed for all possible beam settings, and (2) *the patient dependent* (lower) part which takes the beam shaping modifiers into account. The simulation of the patient independent part can be represented in a comprehensive form by the phase space (PS) information. In case of a full MC simulation of the geometrical model of the accelerator head, the PS information is recorded at a Scoring Plane (SP) placed just in front of the beam modulators. The file containing the PS information recorded in the chosen scoring plane is thereafter used as the particle source for further MC simulation of the patient dependent part of the accelerator and dose calculation in the patient.

The PS file contains information about all particles, including the particles which do not reach the patient due to absorption in or scatter at the beam modifiers, or they have a spacial direction which will remove them from the beam in the next steps of the simulation. Therefore, due to the constant high ratio of "lost" particles with respect to the number of particles emitted from the target, the method of tracking all the particles read from the PS information from scoring planes located in a plane traversed in the initial phase of the transition through a linac head is inefficient, especially for small fields where most particles are absorbed by the beam modifiers. Since the TPS needs approximately 10^8 particles in order to reduce the statistical noise to an acceptable level, the number of particles stored in the phase space file will normally not provide adequate (high enough) statistics. The lack of particles causes artefacts in the dose correlations uncertainties pattern. Another important aspect to take into account concerning full MC simulations is that the commissioning of the accelerator head is cumbersome. It relies on a trial and error approach which involves repeated changes of the initial electron beam parameters and collection of the calculated PS data at the exit of the accelerator head with subsequent dose distribution calculation. If the dose calculation does not agree with the commissioning measurements within certain acceptance criteria, the whole process has to be repeated with adjusted parameters. The process of commissioning of the accelerator head can therefore take days or weeks depending on the required accuracy. Because each accelerator has individual beam properties, it has to be commissioned individually. In order to gain an acceptable efficiency both in modelling of the accelerator head and for the commissioning of it, an effective and accurate beam model is wanted for the MC-TPS.

2.2 A Geometrical BEAMnrc Model of the Accelerator Head for 6 MV and 15 MV photon beams

The program package BEAMnrc is a MC program system introduced by [59] for simulation studies of radiation therapy sources. It is built on the EGSnrc MC code for transport of electrons and photons[7] and according to its license of use, it can be used only for research, and thus, it cannot be directly applied in the clinical routine. BEAMnrc can model all types of medical linear accelerators using its component module system. Each part of the accelerator is regarded as a separate component which can be composed of separate elements defined by geometrical and composition information obtained from the manufacturer. All components together build up the geometrical model of the accelerator head, e.g. primary collimator, flatten-

ing filter, multi-leaf collimator (MLC), jaws etc. (Figure 2.1). BEAMnrc allows for recording the PS information in any number of scoring planes after each accelerator head component.

In the section of Biomedical Physics at University Hospital in Tübingen, Germany, two BEAMnrc models were commissioned for a 6 MV [18] and a 15 MV [54], beam model of the ELEKTA Precise SL*i* linear accelerator. The ELEKTA SL*i* linac has collimators that shape treatment fields from the smallest field size of 1x1 cm^2, to the largest field size of 40x40 cm^2 (the field size is always defined in the isocentre plane), as well as irregular fields shaped by a multi leaf collimator (MLC) and two pairs of jaws. The MLC consists of 40 leaf pairs, each with a projected width of 1 cm at isocentre. The geometrical models are built from the following components: X-ray target, primary collimator, one (6 MV) or two (15 MV) flattening filters, ionization chamber, back-scatter plate, mirror, MLC and X- and Y-jaw pairs (Figure 2.1).

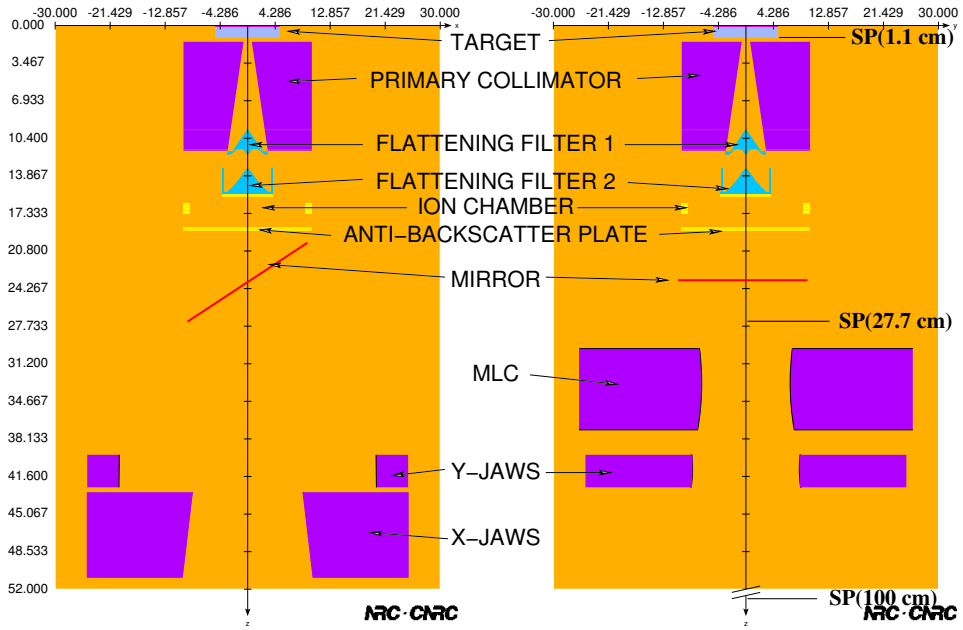

Figure 2.1: The geometrical head model of the ELEKTA SL*i* with indicated BEAM components and the positions of the scoring planes of the PS. Flattening filter 1 is only present in the 15 MV head model.

In this thesis work, PS information for the field size of 40x40 cm^2 for 6 MV and 15 MV beams were recorded in three scoring planes located at: (1) the bottom of the target, SP (1.1 cm); (2) the upper edge of the MLC, SP (27.7 cm) and (3) the isocentre, SP (100 cm) and these 3 planes are referred to as PS (1.1 cm), PS (27.7 cm) and PS (100 cm), respectively (see Figure 2.1).

The applied parameter settings for the BEAMnrc simulations were:

- global electron energy cut-off ECUT = 0.521 MeV for 6 MV.
- ECUT = 0.7 MeV for 15 MV.
- Global photon energy cut-off PCUT = 10 keV for 6 MV and 15 MV.

- No bremsstrahlung splitting.
- No electron or photon range rejection.
- The default EGS4 MC code parameters.
- The number of simulated histories (initial electrons impinging on the target) was set to $5 \cdot 10^8$.

Please notice that the PS data simulated with the BEAMnrc system are not allowed to use clinically according to the BEAMnrc user licence. Therefore, these PS data where never used for treatment planning in our clinic. Only plans created with our VSM were applied after a careful commissioning process.

2.3 BEAM Phase Space data

Phase Space files created with the BEAMnrc code contain all information needed to generate the particles and the information of their key parameters, needed for further MC simulations. When crossing a predefined scoring plane, each particle is recorded as 28 bit data words in the PS file. Each PS entry contains: the kinetic energy (p_x, p_y, p_z), the location in the SP (x, y, z), the direction, the statistical particle weight, and optionally, the place of the last interactions (ZLAST) and the LATCH record. The LATCH record contains information about where a particle had its last interaction. A detailed description of the PS file format can be found in [57].

2.4 Virtual Source Model

The concept of the multiple-source model was introduced by Ma and Rogers[49]. They showed that the particles from different components of a linear accelerator have different energy, angular and spatial distributions. However the particles from the same component have very similar characteristics, in terms of range of energies and incident directions, which are almost independent of their positions on the phantom surface [46]. Therefore, the idea behind the multiple-source model is that particles coming from different parts of an accelerator may be treated as if they are coming from different sub-sources (radiation sources). Looking at Figure 2.1, one can easily distinguish several elements which can be considered as a separate radiation source. Such sources are refereed in literature as virtual source since they do not represent real radiation sources.

In order to parametrize each radiation source for each accelerator component one would have to use many parameters which would make the model difficult to commission and not necessarily better. Therefore, it is practical to define only a few radiation sources which represents the main beam components instead of each accelerator head element. The VSM presented in this work tries to compress PS from the invariant part of the accelerator head into only three sources. These correspond to three main beam components: primary photons, secondary photons and electron contamination.

.

The following sections will aim at explaining the concept of the Virtual Source Model by defining the different (virtual) radiation sources in the head of the accelerator, the location of these sources and all the corrections which need to be considered for accurate representation of the Phase Space information.

2.4.1 Photon beam components

The main components of a photon beam are primary photons, head scattered secondary photons and contamination electrons.The main beam components, sorted after particle type, are defined as follows:

The primary beam component - photons that originate from the bremsstrahlung producing target and which do not interact with any other component of the accelerator head. These photons will hereafter be referred to as primary photons.

The secondary (scattered) photon beam component - contains photons which, by interactions with other components in the accelerator head than the target, change their direction and which will accordingly also, in general, lose energy. This component includes the secondary photons which are created due to bremsstrahlung radiation or pair production induced elsewhere than in the target. For convenience, these photons will hereafter be referred to as secondary photons.

Contamination electrons - are produced by Compton scatter in the accelerator components or in air and contribute to the surface dose. They are an undesirable side product of the photon field, and will therefore be refereed to as contamination electrons.

The dose distribution plotted as a function of where the particles are produced, refereed to as the different beam components (primary, secondary, contamination electrons), shows a different relative contribution to the total dose as well as different properties for the three main components (see Figure 2.2). The primary beam component is the most dominant; it has a sharp field edge (penumbra) which indicates that the primary source has a relatively small diameter. This is also confirmed by the study of the output factors for larger field sizes, this showing that for such an opening, the primary source is fully exposed, as one finds an almost invariant output factor (OF, Equation 6.4) for various larger field sizes This implies that the rather small primary source is not exposed to a greater extent when increasing the field size above a certain value (Figure 2.3). The presented cross profile at shallow depth (Figure 2.2) has a central depression. This is an effect of the flattening filter which is reduced and almost disappears at larger water depths. This phenomena will be explained in more detail in chapter 3.

The contribution from secondary photons to the total dose distribution depends strongly on the field size. It is relatively high for large fields, while for small fields, it becomes negligible (Figure 2.3). The (virtual) penumbra of the secondary cross profile is much broader compared to the primary cross profile. Both of these properties indicate that the secondary photon source has a larger diameter than the primary source. This also explains the fact the secondary output factor drops significantly for relatively large fields sizes while the primary output factor is moderated by very small fields. The slight increase of the primary output factor is caused by the phantom scatter (Figure 2.3). The cross-profile of the secondary photon source lacks distinctive features, indicating a more homogeneous particle fluence then the primary component.

The electron contamination component is similar to the secondary photon beam component with respect to the source size (varying OFs with field size, broad penumbra). The depth dose distribution for electrons is characteristically different than the depth dose curve for the photons, since electrons are directly ionizing particles which deposit energy continuously and are therefore slowed down and stopped close to the surface of the medium they traverse into (Figure 2.2).

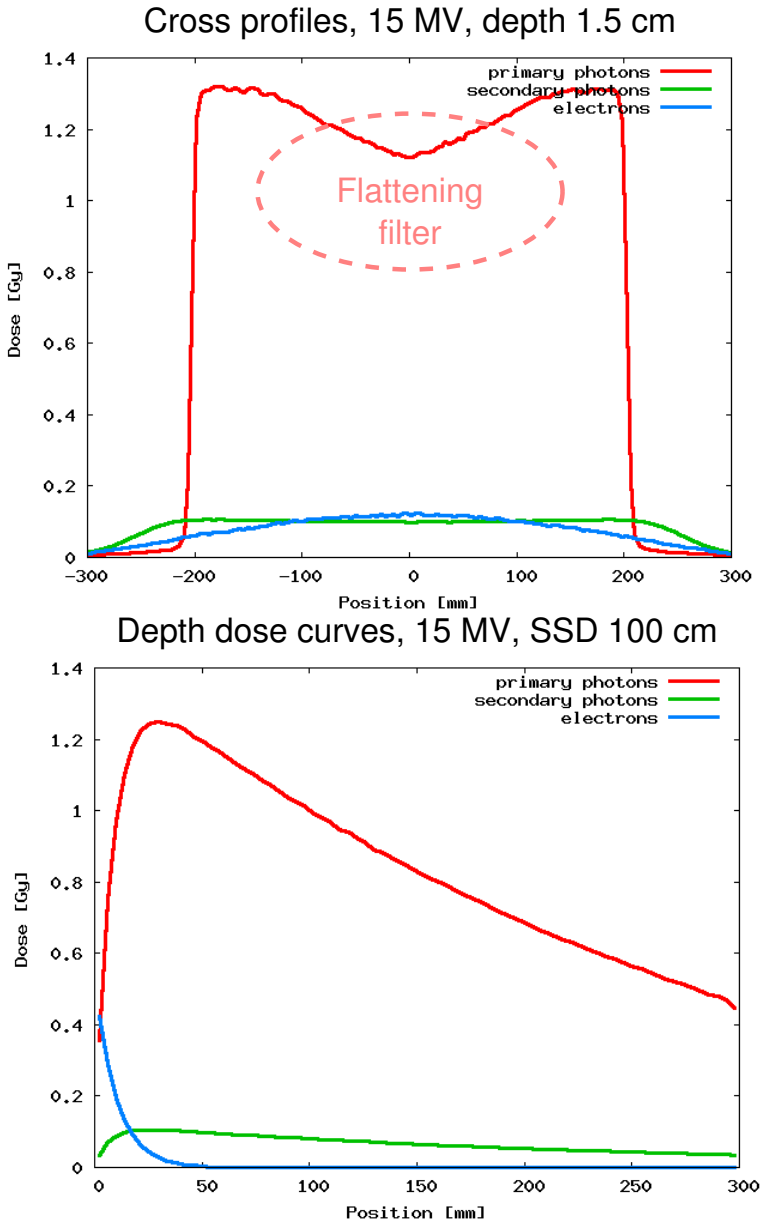

Figure 2.2: Monte Carlo simulations: The relative dose contributions from the 3 main beam components. Cross profiles (upper) and depth dose curves (lower), with the dose distribution for each component shown. Here the field size was set to 40x40 cm^2, the SSD=100 cm and the cross profile is shown for the depth of 1.5 cm in a simulated water phantom. The primary cross profile shows a central depression caused by the flattening filter.

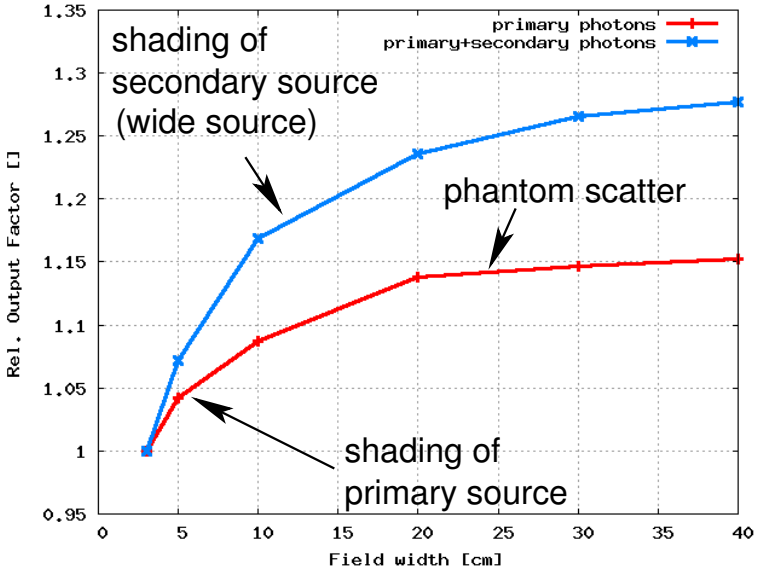

Figure 2.3: Relative change of output factors (15 MV) of the primary and the secondary beam component calculated relative to the delivered dose for a 3x3 cm^2 field size at 10 cm depth and a source-to-surface distance (SSD) of 100 cm.

2.4.2 Photon beam radiation components

The position of each particle's last interaction (ZLAST) is correlated with the location of the components of the geometrical head model (Figure 2.4). The most dominant beam component is the primary photon component ($\approx$ 70%) (Table 2.1). According to the definition of source location, the primary photons originate from the X-ray target and it is presented in Figure 2.4 in ZLAST $\backsimeq$ 0 cm. The secondary photons ($\approx$ 30%) originate from various locations in the accelerator head. Most of the secondary photons originate from the flattening filter, the primary collimator and the anti-backscatter plate. There is also a small radiation source, the SP (30 cm), of backscattered photons from the MLC. The contribution from the primary collimator is more than two times higher for the 15 MV than for the 6 MV beam model. Due to the higher energies of photons in the 15 MV beam, the probability of large angle scattering, or absorption is lower than in the 6 MV beam, so that a larger fraction of scattered photons ends up within the 40x40 cm^2 field. The contamination electrons constitute less than 1.5%, still they are an important source of radiation to model since they contribute significantly to the (skin) dose at the patient surface. There are three main electron sources: the flattening filter, the anti-backscatter plate and the MLC. No contamination electrons from above the flattening filter reach the patient dependent part of the accelerator.

2.4.3 Phase Space information represented by Virtual Sources

The basic idea of the VSM is to model the invariant part of the accelerator head by satisfying the following demands: (1) the behaviour of the model must be transparent and simple enough, and have a minimum number of free parameters, (2) the free parameters should be determined by measurements which are not too complicated, error-prone or time consuming, for easy and

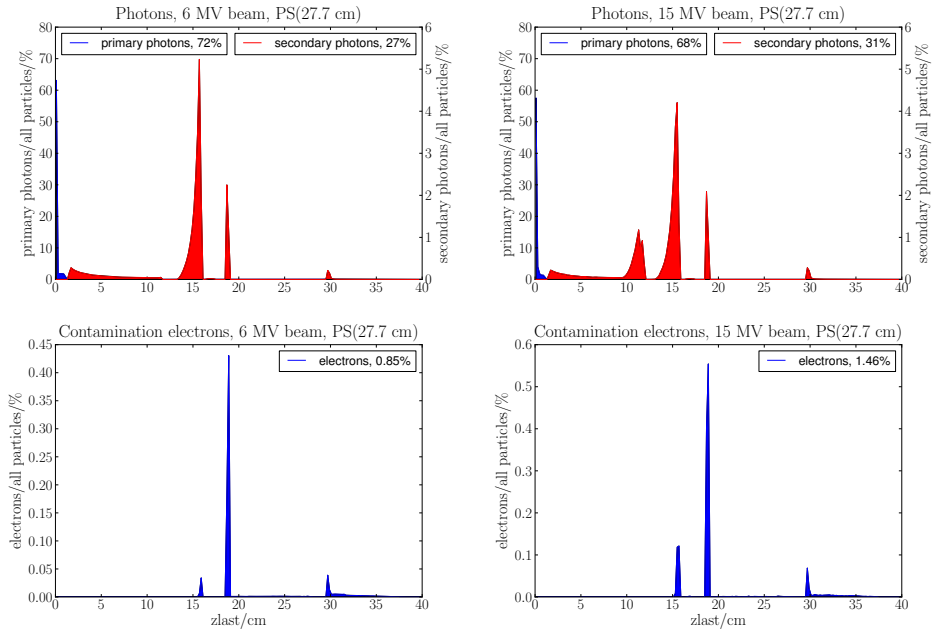

Figure 2.4: Particle percentage statistics with respect to the last interaction location in the accelerator head for 6 MV (left column) and 15 MV (right column) for primary and secondary photons (upper row) and contamination electrons (lower row). Results based on the PS (27.7) both for the 6 MV beam and the 15 MV beam.

robust commissioning, (3) it should be comprehensive enough to confirm with the accuracy demands for all field sizes between field sizes smaller than 1x1 cm^2 up to 40x40 cm^2 and (4) it should be numerically efficient which means that a minimum number of operations needs to be performed in order to generate particles.

All the three main beam components have different PS properties which will result in different dose distribution properties (Figure 2.2). Therefore, it can be argued that it is reasonable to describe each of them as a separate virtual source. The primary source is well defined with respect to location. However, the location of the virtual sources for the secondary photons and the contamination electrons are more difficult to define because they consist of several radiation sources, all coming from the different elements of the accelerator head (Figure 2.2). This work will show how it is possible to compress all PS of the invariant part of the accelerator into the three described virtual sources: (1) the primary photons, (2) the secondary photons and (3) the contamination electrons.

When a distribution of particles undergoing different physical processes which produces the particles of interest in a certain category are grouped together as originating from a particle source, the properties of this source can naturally become quite complex. For example, the probability P that a particle of type (e^-, X) and energy E is emitted into the spacial angle $\vec{\Omega}$, will depend on its position of emission $\vec{x}$. Hence, the emission probability P(E, $\vec{x}$, $\vec{\Omega}$) of a virtual source is a function with five variables.

Throughout this work, it is hypothesized that the probability factor P is expressed as

$$P(E,\vec{x},\vec{\Omega}) = p(E,\vec{\Omega}) \cdot \Sigma(E,\vec{x}) \cdot \Phi(\vec{\Omega}) \tag{2.1}$$

Table 2.1: Relative particle count of the beam components and relative contribution of the secondary photons interacting with the geometrical head components.

Phase Space, SP(27.7 cm)	*Beam 6 MV [%]*	*Beam 15 MV [%]*
Beam components		
Primary photons	72	68
Secondary photons	27	31
Contamination electrons	0.85	1.46
The Secondary photons are interacting with		
Primary collimator	4.4	9.8
Flattening filter	18.6	17.3
Anti-backscatter plate	3.4	3.2
Rest (ion chamber, mirror, MLC)	0.6	0.7

where:

p is the energy spectrum,
Σ is the source emission density,
Φ is the particle fluence correction.

Throughout this work, the sources are assumed to be radially symmetric, hence

$$\Sigma(E,\vec{x}) = \Sigma(E, \|\vec{x}\| = r) \tag{2.2}$$

PS data evaluations at arbitrary locations

In order to determine the corrections depending on $\vec{\Omega}$, it proves helpful to investigate PS properties at other locations then the original scoring plane.

A new PS can be calculated by geometrical tracing of particles from the original PS to a plane position using their directional vector and the location parameters are stored stored in the PS in front of the beam modulators.

Definitions of Virtual Sources

- The primary photon source is in reality and by definition located in the bremsstrahlung producing target, SP(0 cm), and this source has a Gaussian distribution with no energy dependence $\sigma_{pri}(r)$.
- The secondary source is defined to be located at the base of the primary collimator, and this source has a Gaussian energy dependent spatial distribution $\sigma_{sec}(E,r)$.
- The electron contamination source is defined to be located at the base of the second flattening filter and it has a Gaussian energy dependent spacial distribution defined by $\sigma_{econ}(E,r)$.

The primary source $\sigma_{pri}(r)$ is evaluated through commissioning measurements, especially by the use of results from measurements with small fields. The sources $\sigma_{sec}(E,r)$ and $\sigma_{econ}(E,r)$ are derived from the BEAMnrc PS reconstructed at the source plane position by back projection of the PS(27.7 cm). The back projection of the PS(27.7 cm) to this source plane was performed with a tool developed by the author (Chapter 6, Appendix B).

All sources have an energy spectrum which is described by analytical functions derived from PS analysis and these are described in the following chapters. The angular distribution

results from the location and extent of the source and the particle fluence distribution Φ of the sources.

Correction for Phase Space Characteristics

The PS file contains information about characteristic phenomena of the beam component they represent, such as the off-axis energy spectrum softening, the energy fluence etc. We therefore chose to let the VSM employ the following corrections for various PS characteristics:

- off-axis energy softening for primary and secondary photons,
- absorption/scatter in the flattening filter,
- energy fluence normalization,
- energy fluence flatness and particle fluence central depression for primary photons,
- correction for energy-focussing of the source distribution for secondary photons and contamination electrons,
- enhancement of the focus spot particle fluence for contamination electrons.

These corrections are described in detail in chapters 3, 4 and 5.

Phase Space Reconstruction

A beam model has an algorithm to represent the PS information as well as an algorithm to reconstruct it. In our model the PS is represented by virtual sources defined in Section 2.4.3and described in following chapters 3, 4, 5.

In the VSM the PS information is reconstructed in the following way:

1. The first step is to select randomly a source between primary, secondary and contamination souce according to the relative source intensity which corresponds to primary, secondary and electron contamination contributions of the VSM as described in Section 6.2.
2. The energy and location in the source plane are sampled from the energy spectrum $p(E,\Omega)$ and the particle source distribution $\Sigma(E,r)$.
3. The initial direction of the generated particle is determined by sampling of a location in the scoring plane located in front of the beam modulators from a uniform distribution.
4. The statistical weight is changed depending on the correction models e.g. flatness correction, energy fluence normalization, the flattening filter model etc. (Section 2.4.3).
5. The particle is now ready for further MC simulation through the beam modulators and into and within the patient.

2.5 Beam modulators - patient dependent elements

A time consuming part of the MC simulation is the transport of particles through the beam modulators (MLC, jaws, wedges) and many particles are lost while traversing thick, high-Z, materials, due to absorption and scatter. This is the case especially for small fields where a large area of the field is blocked and only a small fraction of the simulated particles reaches the patient. In order to shorten the time of simulation, an efficient model of the beam modifiers is desirable. Therefore, probabilistic models of the beam modifiers have been proposed by several authors [65, 11, 35]. In this work, a Transmission Probability Filter was employed to model the beam modifiers.

The main advantages of using a Transmission Probability Filter (TPF) instead of direct MC simulation of particle transport through the beam modifiers are: (1) it is much faster, since the TPF calculates the probability of a particle transition through a certain region of the linac head, (2) it is tunable based on standard dosimetric measurements in order to represent the individual properties of the beam modifiers, and (3) it does not require comprehensive information about the linac head geometry.

The basic idea of the TPF is to transform the three-dimensional (3D) geometry of the beam modifiers into a 3D transmission map. The TPF elements are characterised by their geometric and probabilistic parameters. The geometric parameters define the real dimensions and the extent of the secondary collimator (SC) elements, while the probabilistic parameters define the transmission probabilities for the particles with respect to their traversing through the beam modifier elements, see Table 2.5.

The geometrical parameters (Table 2.5) are different for each type of collimation system. Therefore, the TPF requires the basic geometric parameters like the width and thickness of the collimation system elements. This information can be obtained from the technical documentation of the collimation system or from the vendors and from the literature.

The probabilistic parameters describe the transmission probability of the TPF elements, these are obtained from dosimetric measurements, MC simulations or through available literature. Many investigators provide experimental data on the dosimetric properties of the beam modifiers (secondary collimators) of various accelerator types by measurements of the MLC and jaw transmission [30, 27, 8, 44, 26, 56].

Table 2.5 shows the results of a tuning of the TPF parameters for two types of MLC, namely a beam modulator (BM) with a 0.4 cm leaf width, and a MLC with a standard leaf width of 1 cm (MLCi). The BM has no Tong&Groove (T&G) design to prevent radiation to leak between the leaves like the MLCi has. Instead, the leaf bank is tilted to block the primary particles from passing between the leaves. Moreover, the BM has no jaws to reduce the radiation passing through the leaves. Due to this, an increased amount of radiation passes through the leaves (1%) and between the leaves (1.7%) with the BM[56] design.

Table 2.2: Transmission Probability Filter model: The geometric and probabilistic parameters of the Beam Modulator (BM) and MLCi collimation systems. The letters T (Transversal) and P (Parallel) indicate the direction of the jaw movements relative to the MLCs movement direction.

Geometrical parameters	BM	MLCi	Probabilistic parameters	BM	MLCi
number of leaves	40	40	interleaf factor,T_{inter}/%	5.0	10.0
leaf width @ iso/mm	4	10	leaf transmission, T_{leaf}/%	0.006	0.012
T&G design	NO	YES	groove width, $T\&G$/mm	0.6	1.0
inter-leaf gap/mm	∼0.1	∼0.1	leaf tip factor, T_{tip}/%	1.2	1.15
MLC plane position/mm	390.3	298.5	T-jaw transmission, T_{tjaw} /%	–	0.012
T-jaw plane position/mm	470†	431	P-jaw transmission, T_{pjaw}/%	–	0.103
P-jaw plane position/mm	470†	394			
max. T-jaw retraction/mm	80	200			
max. P-jaw retraction/mm	105	200			
T-jaw thickness/mm	-	78			
P-jaw thickness/mm	-	30			
leaf thickness/mm	75	75			
leaf tip shift/mm	-0.2‡	0.0			

† fixed frame

‡ individual value for UKT accelerator (default 0 mm)

Chapter 3

The Primary Photon Beam Component

3.1 General considerations and BEAM analysis

The primary electron beam impinging on the high-Z metal target produces bremsstrahlung photon radiation when hitting the target. For high energy electrons, the average bremsstrahlung photon emission angle is approximately given by $\frac{m_0c^2}{E}$, where m_0c^2 is the electron rest energy and E its total energy, resulting in a strongly forward-peaked angular distribution (Figure 3.1). The resulting photon intensity has a forward peaked angular distribution, and the angular distribution is strongly anisotropic, while the photon energy spectrum has a weak angular dependency [77]. In particular, high photon energies occur slightly less frequent if the photon is emitted at an angle to the beam axis due to inelastic collisions of the electron before the bremsstrahlung emission.

The bremsstrahlung radiation is modified by the flattening filter such that the beam gets a flat energy fluence which results in a flat dose distribution for field sizes up to 40x40 cm^2 at depths between 5 and 25 cm. To achieve this, the flattening filter has its greatest thickness in the center and the thickness decreases gradually with increasing distance outwards from the central axis. This produces a particle fluence with a central depression (Figure 3.2 and Figure 3.1), especially at shallow depths. The central depression of the particle fluence decreases as the depth increases.

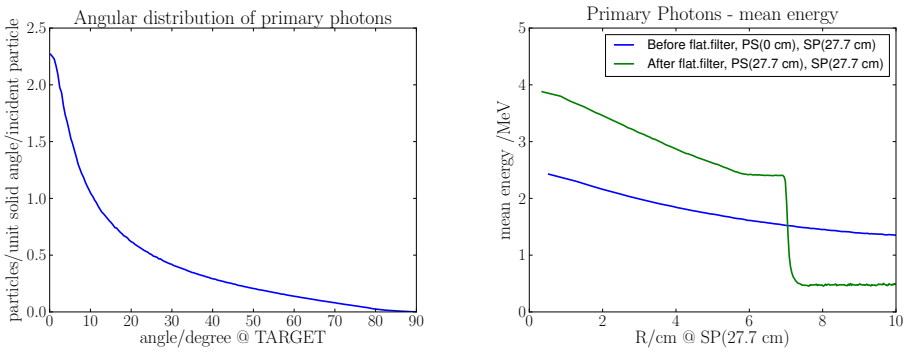

Figure 3.1: The primary photon angular distribution before the flattening filter (left). The change in mean energy is due to the presence of the flattening filter (right) due to a differential absorption of lower energy photons. Results are shown for the 15 MV BEAM model.

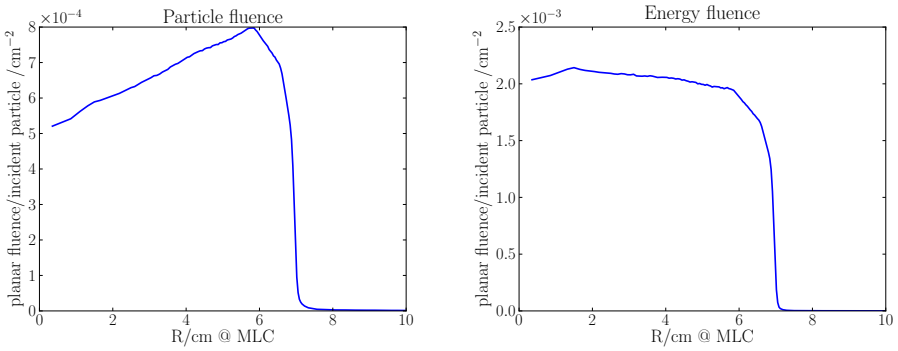

Figure 3.2: The primary photon particle fluence and energy fluence calculated at SP(100cm). Results are shown for the 15 MV BEAM model.

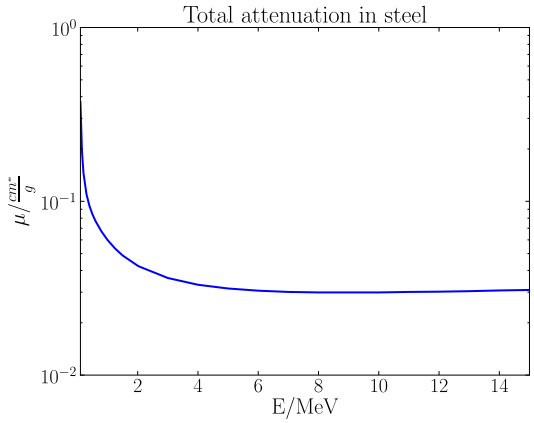

Figure 3.3: The total steel attenuation coefficient with respect to photon kinetic energy. Data retrieved from NIST Standard Reference Database 8 (XGAM).

The flattening filter in Elekta linacs is normally made of steel. The total attenuation coefficient for photons in steel, as in all other materials, depends on the kinetic energy of the traversing photons. As Figure 3.3 shows the cross section for photon attenuation in steel is larger for low energy photons than for photons with higher energy, i.e. the flattening filter attenuates low energy photons more efficiently than higher energy photons. This results in a so-called spectrum hardening effect which increases the mean energy of the photon beam (Figure 3.1, right panel). Since the effective thickness of the flattening filter varies with distance from the central axis, the effect of the flattening filter on the primary photon beam is differential; this is referred to as an off-axis softening effect. This causes a decrease in the primary mean energy with increasing distance from the central axis (Figure 3.4).

The primary photon beam before and after the flattening filter were analysed based on PS files at the SP(1.1 cm) (just after the target) and SP(27.7 cm). The PS(1.1 cm) was geometrically projected to the scoring plane SP(27.7 cm) using the direction and location of particles from the PS(1.1 cm). The primary photon energy spectra were compiled in radial bins. Each radial bin was defined as the cross section of SP(27.7 cm) with one inner and one outer cone,

both located with the vertex at the beginning of the central axis and with a constant angle of three degrees between the cone walls.

The BEAMnrc analysis confirms that the primary photon energy spectra vary weakly with the radial bins (Figure 3.4, upper). After the flattening filter (Figure 3.4, lower) one sees a more pronounced off-axis softening effect (i.e. the energy spectra of the radial bins get softer with increasing distance to the central axis) as well as the beam hardening effect (i.e. the mean energies are shifted towards higher energies after the flattening filter). These phenomena are represented in the VSM by the off-axis softening before the flattening filter of the primary energy spectrum and the differential attenuation model of the flattening filter.

3.2 VSM representation

3.2.1 Source location

Bremsstrahlung photons that are produced in the high-Z target by primary electrons in this energy range (MeV), originate for the most part from a relatively thin layer at the top of the target [77]. Therefore, the primary source is located at SP(0 cm) which is also the location of the primary Gaussian source in the VSM.

3.2.2 The Primary Photon Energy Spectrum

The primary photon spectrum, $p_{pri}(E)$, describes the energy distribution of the primary photons above the flattening filter (Figure 3.6, upper) which is later modified by the energy-dependent absorption in a phenomenological model of the flattening filter (sec.3.2.4) (Figure 3.6, lower). The spectrum $p_{pri}(E)$ is described by a composed function (3.1) defined in two energy ranges. The low energy range between the energy cut-out (E_{cut}) and the minimum energy (E_{min}); and the energy range E_{cut} between the E_{min} and the maximum energy (E_{max}):

$$p_{pri}(E) = \begin{cases} w_o & , E_{cut} \leq E < E_{min} \\ \left(\frac{E}{E_{max}}\right)^{-b_{pri}} - 1.0 & , E_{min} \leq E \leq E_{max} \end{cases} \tag{3.1}$$

It is recommended to set the E_{min} equal to 0.511 MeV - the energy of annihilation photons. Then, low energetic primary photons ($E_{cut} < E < E_{min}$) are modified by a free parameter (w_o) and primary photons with a higher energy ($E \geq E_{min}$) are described by an analytical function with a reference parameter b_{pri}. The b_{pri} is evaluated based on the PS recorded after the X-ray target (before the flattening filter), the PS(1.1 cm). For the 6 MV and 15 MV models b_{pri} values are 1.05 and 0.76, respectively (Figure 3.5).

3.2.3 Off-axis energy spectrum softening before flattening filter

The relative change of the mean energy of the primary photon spectrum before the flattening filter, $p_{pri}(E)$, is modelled by an effective change in $b_{pri}(\nu)$ with respect to the tangent of the angle between the direction of the particles and the central axis ($\tan(\nu)$). The change in $b_{pri}(\nu)$ as a function of $\tan(\nu)$ is tuned by δb_{pri}:

$$b_{pri} = b_{pri} - \delta b_{pri} \tan(\nu) \, , \delta \mathrm{b_{pri}} > 0, \tag{3.2}$$

which is fixed for a given beam model. These parameters are derived from PS(1.1 cm) data analysis of the BEAMnrc PS recorded above the flattening filter. For the 6 MV and the 15 MV beam model δb_{pri} is to be 0.62 and 1.03, respectively.

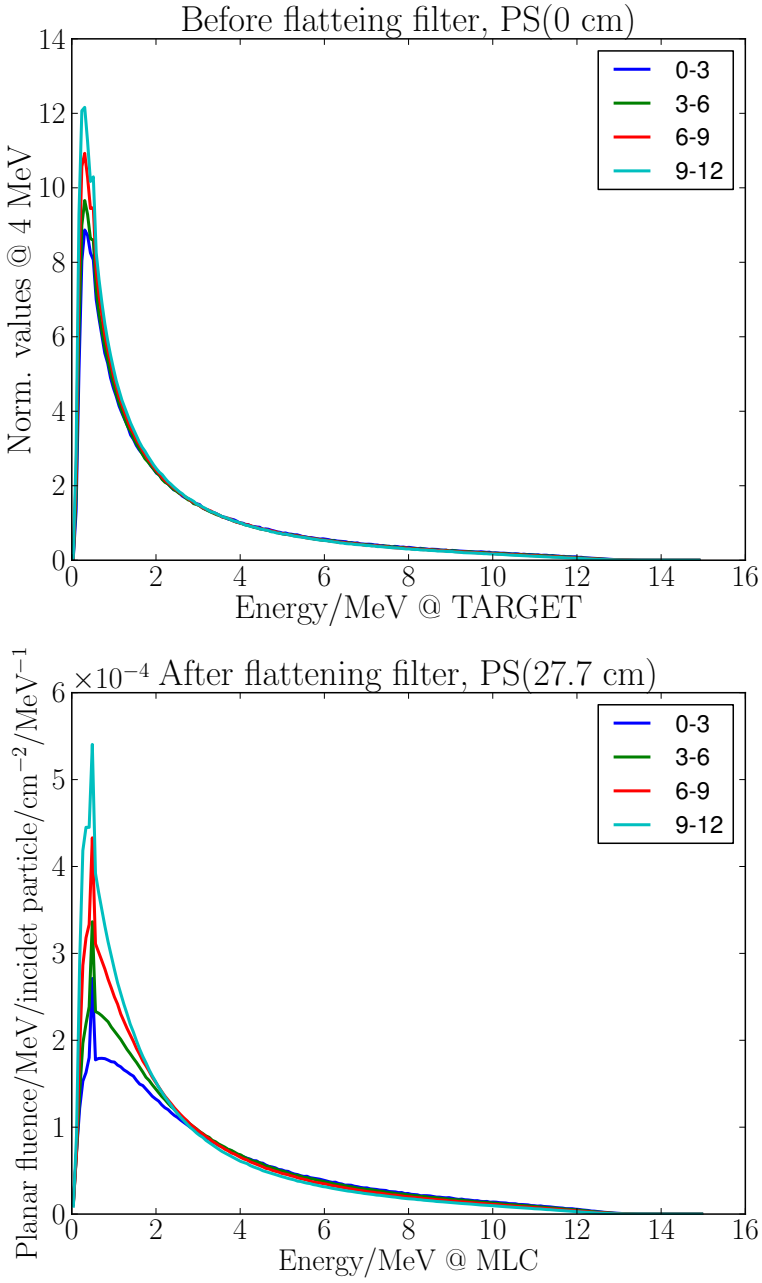

Figure 3.4: Off-axis softening of the primary photon spectra due to the differential effect of the flattening filter. Primary photon spectra above (upper) and below (lower) the flattening filter calculated for the radial bins: 0-3 degrees (blue), 3-6 degrees (green), 6-9 degrees (red) and 9-12 degrees (cyan). The presented results were obtained for the 15 MV BEAM model.

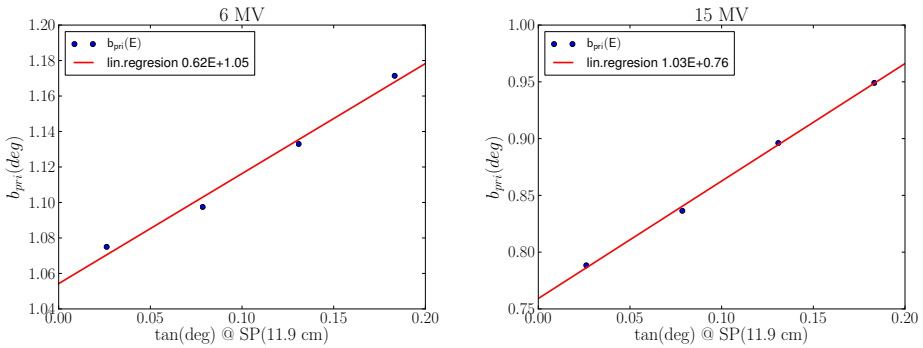

Figure 3.5: Off-axis parameter fitting of the primary spectrum: $b_{pri} = 1.05$ and $\delta b_{pri} = 0.62$ (left) and $b_{pri} = 0.76$, $\delta b_{pri} = 1.03$ (right) for the 6 MV and 15 MV beam models respectively.

3.2.4 A model for attenuation in the flattening filter

The model of how the flattening filter modifies the primary photon energy spectrum (Equation 3.1) has its aim in mimicking the differential effects of beam hardening and off-axis energy softening. For that, the VSM employs a flattening filter correction function, $f(\mu,t)$, which describes the effect of the energy-dependent attenuation of primary photons (Figure 3.3). The function $f(\mu,t)$ is described by

$$f(\mu(E),t(d,r,h)) = \rho\ \mu(E)\ t(d,r,h) \tag{3.3}$$

where E [MeV] is the primary photon energy, $t(r,d,h)$ [cm] is the effective thickness of the flattening filter as given by the conical shape of the flattening filter, ρ $\left[\frac{\text{g}}{\text{cm}^3}\right]$ is the density of the flattening filter, and $\mu(E)$ $\left[\frac{\text{cm}^2}{\text{g}}\right]$ is an empirical function representing the attenuation coefficient in steel (Figure 3.3):

$$\mu(E) = 0.027\ (E+0.16)^{-1.2} \tag{3.4}$$

The flattening filter correction function, $f(\mu,t)$, modulates the primary spectrum before the flattening filter, p_{pri}, to produce the primary photon spectrum after the flattening filter $p'_{pri}(E,r)$:

$$p'_{pri}(E,r) = p_{pri}(E)\ e^{-f(\mu(E),t(d,r,h))} \tag{3.5}$$

This purely phenomenological model requires an effective thickness of the flattening filter, $t(d,r,h)$. The effective thickness of the flattening filter is described by a geometrical function, $t(d,r,h)$, which is parametrized by the maximum effective thickness on the central axis, d [cm/MV], the radius of the location of particle transit, r [cm], and the minimum thickness of the flattening filter h [cm/MV] (Figure 3.7). The maximum effective thickness, d, can be approximated as $d = 3 \cdot E_n$, where E_n is the nominal beam energy. The model does not distinguish between transmission without interaction and small angle scatter. Photons which are scattered with a large scattering angle, i. e. the situations where a photon loses the information about the primary photon original location, and most likely will lose energy due to Compton scattering, have to be represented by a secondary source in the Virtual Source Model (Chapter 4).

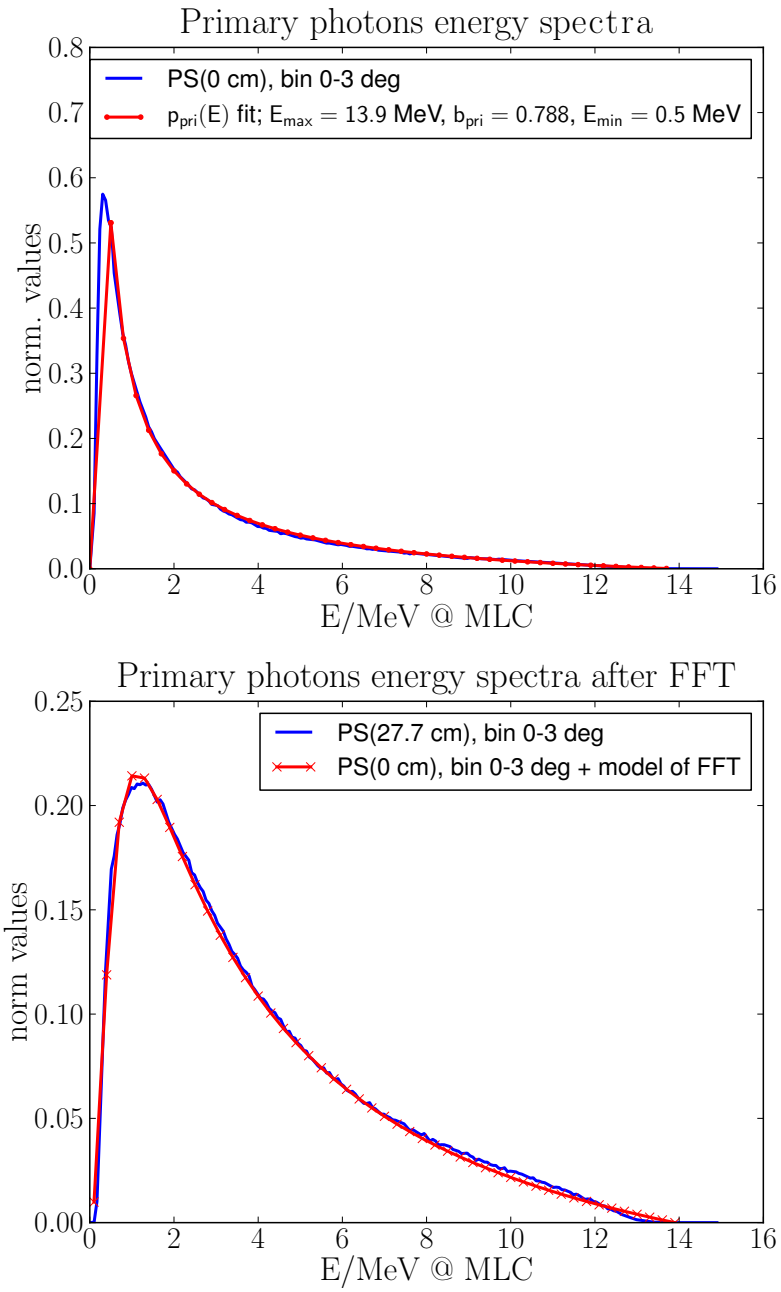

Figure 3.6: Example of a fit of the primary photon spectrum $p_{pri}(E)$ (Formula 3.1) to the PS(0 cm) data of the 15 MV beam model (upper plot) and the effect of the flattening filter correction function (Formula 3.5) (lower plot).

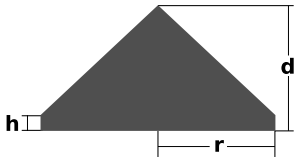

Figure 3.7: The geometrical model of the flattening filter with three adjustable parameters d, r, h.

The correction function, $f(\mu,t)$, (Equation 3.3) has to be incorporated in the primary photon kernels calculation (Chapter 6). The secondary photon spectrum (Equation 4.1) describes the secondary photon energy after the flattening filter, so that the flattening filter correction function, $f(\mu,t)$, does not affect the secondary photons' polyenergetic kernels. The concept of polyenergetic kernels is described in more detail in Chapter 6.

3.2.5 Energy fluence normalization

The flattening filter is designed for to obtain a flat energy fluence and consequently a flat dose distribution for the radiation fields in order to enable a homogenous dose distribution within the irradiated volume. The energy fluence normalization changes the relative weight of primary photons passing through the flattening filter. Without this normalization, the number of primary photons with unit weight would decrease with the effective thickness of the flattening filter, and the energy fluence would increase with the distance from the central axis. This is corrected for by the energy fluence normalization(w_{EFN}):

$$w_{EFN}(r) = \frac{\overline{E_{pri}(r)}}{\overline{E_{pri}(0)}}, \tag{3.6}$$

where $\overline{E_{pri}(r)}$ at the position ,r, in the source plane is described by

$$\overline{E_{pri}(r)} = \frac{\int_0^{E_{max}} E\ p'_{pri}(E,r)\ dE}{\int_0^{E_{max}} p'_{pri}(E,r)\ dE}. \tag{3.7}$$

The energy fluence normalization provides a correction of the statistical weight of each photon and is applied only to the primary photon component.

3.2.6 Lateral enhancement of the energy fluence

The shape of the flattening filter is more complex than described by our analytical model. A precise description of the geometry of the flattening filter would be quite impractical because of the large number of different designs. The deviations from perfect flatness and the central depression phenomena are therefore modelled by a lateral enhancement of the energy fluence of the primary photons. This is described by a Padé function with 5 coefficients,$h_{i,i=0,\ldots,4}$, normalized to the highest order coefficient:

$$h(r) = 1.0 + \frac{h_0 + h_1 r + h_2 r^2 + h_3 r^3 + h_4 r^4}{10^{-4} + h_4 r^6} r^2, \tag{3.8}$$

where r is the position of the photon in the scoring plane SP(27.7 cm).

This correction is implemented such that it does not influence the central axis energy distribution. It is symmetric and it only enhances the off-axis energy distribution by changing the primary photon weight relative to the weight at the central axis.

Section 6.4 demonstrates a fit example of the lateral enhancement coefficients $h_{i,i=0,\ldots,4}$.

3.2.7 The Photon Fluence Distribution

The primary photon fluence distribution, Φ_{pri}, can be assumed to be fairly well represented by a Gaussian distribution, because the origin of the particles is well delimited by the electron beam in the bremsstrahlung producing target:

$$\Sigma_{pri}(r) = \frac{1}{2\sqrt{\pi}} e^{-\frac{r^2}{2\sigma_{pri}^2(E)}}, \tag{3.9}$$

defined by the source size, σ_{pri}. The initailal value of $\sigma_{pri} \approx 0.1$cm is adjusted during commissioning for an individual linear accelerator (Chapter 6).

In order to reconstruct the primary photon fluence, the particle locations, r(0 cm) and r(27.7 cm), are sampled in the primary photon source plane and in the scoring plane above the MLC from $\Phi_{pri}(r)$ and from a uniform distribution, respectively. These two locations determine the initial direction of the generated photon. The remaining particle properties, like the energy and the statistical weight are determined from the primary energy spectrum while applying the angular-dependent corrections (i.e. the model of the flattening filter, the off-axis softening, the energy normalization and the lateral enhancement of the energy fluence).

Chapter 4

The Secondary photon beam component

This chapter aims at explaining how the secondary photon beam component can be represented by one virtual source. Further it aims at describing how the modelling of an off-axis dependent energy spectrum is done and what that is done for this model to have an energy spectrum with off-axis corrections of the particle distribution.

4.1 General consideration and BEAM analysis

In contrast to the primary source, the location of the secondary source is less well defined since it combines a number of scatter sources in the accelerator head. Because the flattening filter and the primary collimators are the main contributing elements to this source, the position of the virtual secondary photon source is chosen to be between the base of the primary collimator and the base of the flattening filter, which in the current accelerator design, co-inside at 11.9 cm measured from the target at 0 cm.

As for the primary photon beam component, the PS(27.7 cm) recorded at the exit of the invariant part of the accelerator for 6 MV and 15 MV beam models were used to analyse the secondary source properties. The common properties of the secondary beam component are in the following presented based on only the 15 MV BEAM PS, i.e. the 6 MV BEAM PS beam properties will not be described here. The secondary photon particle fluence distributions from the PS(27.7 cm) were calculated at SP(27.7 cm) and at SP(11.9 cm); the secondary source plane position. Both particle fluence distributions can be well represented by Gaussian distributions (see Figure 4.1).

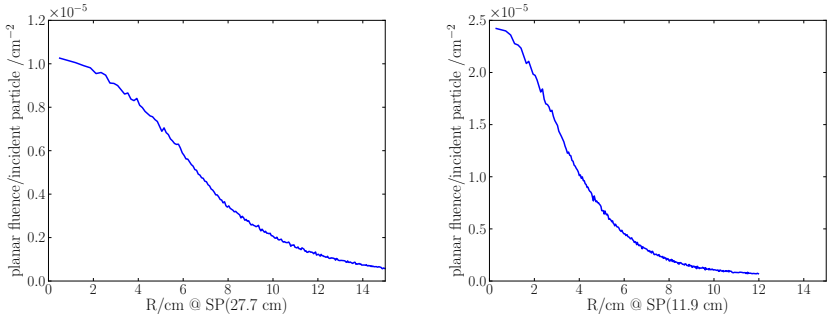

Figure 4.1: Secondary photons particle fluence distributions calculated from the 15 MV PS(27.7 cm) at the SP(27.7 cm) (left) and the source plane position SP(11.9 cm) (right).

The mean energy of the secondary photons is lower than that of the primary photons. The mean energy decreases with the distance from the central axis since particles with larger angle scatter events have transferred more energy than particles with smaller angle scatter events (Figure 4.2). This is more pronounced at the source plane position SP(11.9 cm) than at SP(27.7 cm) because of the different origins of these photons in this plane. Another characteristic feature of the secondary photon spectra is the annihilation peak at 0.511 MeV (Figure 4.2).

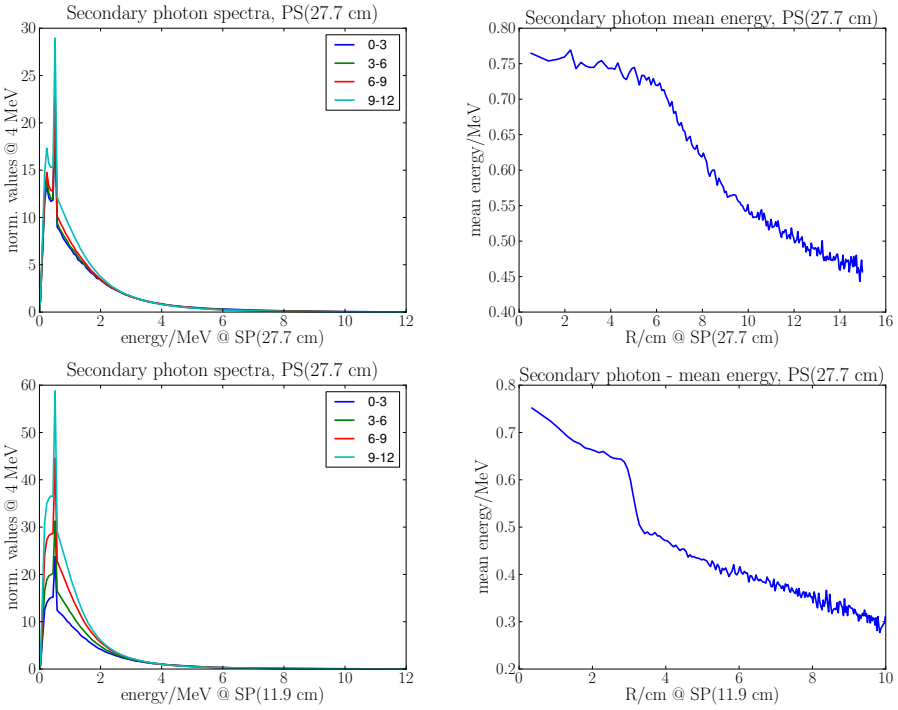

Figure 4.2: Secondary photon spectra (left column) and mean energy of secondary photons with respect to the off-axis position (right column) calculated at the upper edge of the MLC, SP(27.7 cm), (upper row) and recalculated (see section 2.4.3) at the secondary photo plane position, SP(11.9 cm), (lower row). All plots are calculated based on the same PS(27.7 cm) file simulated for the 15 MV photon beam.

4.2 VSM representation of the secondary photon beam component

4.2.1 Source location

In section 2.4.2 it was shown that the secondary photons have no only one specific source (i.e. they originate mainly form the primary collimator, the flattening filter and the anti-backscatter plate, Figure 2.4). Instead of describing the secondary photons originating from many sources, we decided to device a secondary source model where it is assumed that all secondary particles

originates from one virtual source, and then apply corrections to reproduce the angular distribution of the particle fluence and the energy fluence of the BEAMnrc PS data. The position of the secondary source is selected to be positioned at the base of the primary collimator. This is the first place where one can study the secondary particles which has undergone head scatter interactions. Secondary particles created above the primary collimator are either absorbed by the primary collimator or scattered in the direction of the beam, this implying that their angular distribution cannot be distinguished from the secondary photons created at the base of the collimator.

4.2.2 The secondary photon spectrum

The secondary photon spectrum, $p_{sec}(E)$, is described as it appears after the flattening filter, and the flattening filter correction is therefore not applied. As for the primary photon spectrum, $p_{sec}(E)$ is defined in two energy ranges:

$$p_{sec}(E) = \begin{cases} w_s & ,E_{cut} \leq E < E_{min} \\ e^{-b_{sec}E} - e^{-b_{sec}E_{max}} & ,E_{min} \leq E \leq E_{max}, \end{cases} \tag{4.1}$$

where the probability w_s is a free parameter for energies between E_{cut} and E_{min}. E_{min} is set to 0.511 MeV which corresponds to the annihilation peak of the secondary photon spectrum resulting from pair production in the accelerator head elements. Energies between E_{min} and the maximum energy, E_{max}, are described by a function which depends on two free parameters of the VSM; b_{sec} and E_{max}. Please, notice that the maximum energy, E_{max}, is the same for the primary photon source and the secondary photon source and it is defined by the same parameter of the VSM. The maximum energy Emax, is the maximum photon energy in the bremsstrahlung spectrum.

4.2.3 Off-axis energy softening

As for the primary photon spectrum, an off-axis correction of the energy spectrum is necessary. The relative change of $p_{sec}(E)$ with respect to the tangent of the angle between the particles and the central axis, $\tan(\nu)$, is described by:

$$b_{sec} = b_{sec} - \delta b_{sec} \tan(\nu) \, , \delta b_{sec} > 0, \tag{4.2}$$

where δb_{sec} is determined by fitting of δb_{sec} for each radial bin calculated for BEAMnrc PS(27.7 cm). The results from this fit show a linear dependence between δb_{sec} and $\tan(\nu)$, with δb_{sec} equal to 1.43 and 1.99 for the 6 MV and 15 MV BEAM model, respectively (Figure 4.3).

4.2.4 An energy-focussed fluence distribution.

The main sources of the secondary photon radiation are: 1) coherent and incoherent scattering of primary photons on elements of the accelerator head, 2) bremsstrahlung radiation emitted through secondary electron interactions with a nucleus, 3) characteristic X-ray radiation caused by transitions of orbital electrons, and 4) annihilation radiation emitted through orbital electron annihilation. The major part of the interactions in the accelerator head originates from scatter and bremsstrahlung radiation. The probability of coherent (Rayleigh) and incoherent (Compton) scattering decreases with photon energy. In case of bremsstrahlung radiation, the photon emission angle decreases when the electron energy increases (see Section

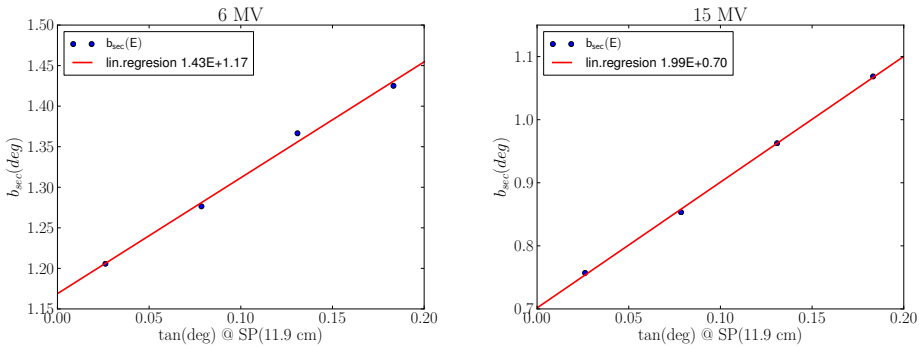

Figure 4.3: Off-axis parameter fitting of the secondary spectrum for the 6MV beam model: $b_{sec} = 1.17$, $\delta b_{sec} = 1.43$ (left), and the 15 MV beam model: $b_{sec} = 0.70$, $\delta b_{sec} = 1.99$ (right), respectively.

3.1). This explains why the apparent source distribution of the secondary beam component depends on the kinetic energy of the secondary photons. This phenomena will be referred to as an *energy-focussed distribution* of the secondary source.

The energy-focussed distribution of the secondary source is demonstrated in Figure 4.4 (left plot) and 4.5 (left plot) where the particle fluence is calculated in incremental 1 MeV energy bins from the BEAM PS(27.7 cm) projected to the secondary source plane - SP(11.9 cm). The result of the calculation clearly demonstrates a decrease of the secondary source size with energy. The shape of the particle fluence distribution for each energy bin follows the Gaussian distribution with a rapid horn-drop at R≈ 3.3 cm which corresponds to the projected radius of the primary collimator opening for the SP(11.9 cm). Most of the secondary photons generated by the VSM from the secondary source beyond R≈ 3.3 cm will get a tangential direction with respect to the central axis. Most of them will be removed from the beam by the further beam modulators (jaws, MLC), especially for small to mid-sized fields. Therefore, the discrepancies between the BEAMnrc particle fluence and the VSM secondary source particle fluence in the outward region (R>3.3 cm) are neglected.

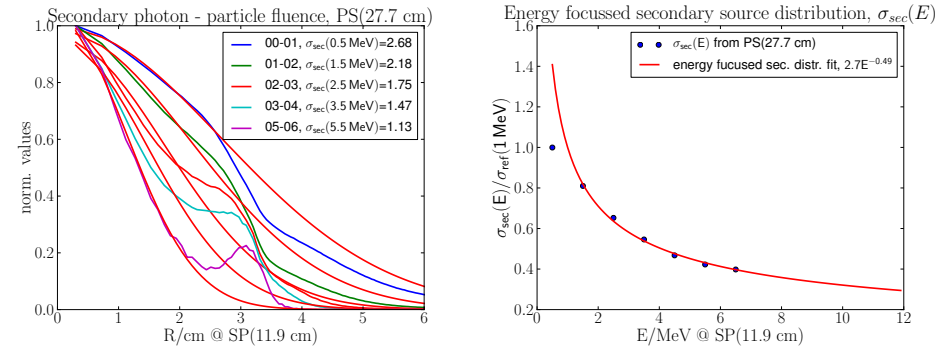

Figure 4.4: Left: The 6MV energy-focussed distribution of the secondary source with the Gaussian fit of its particle fluence calculated in the energy bin. Right: the fit of $\sigma_{sec}(E)$.

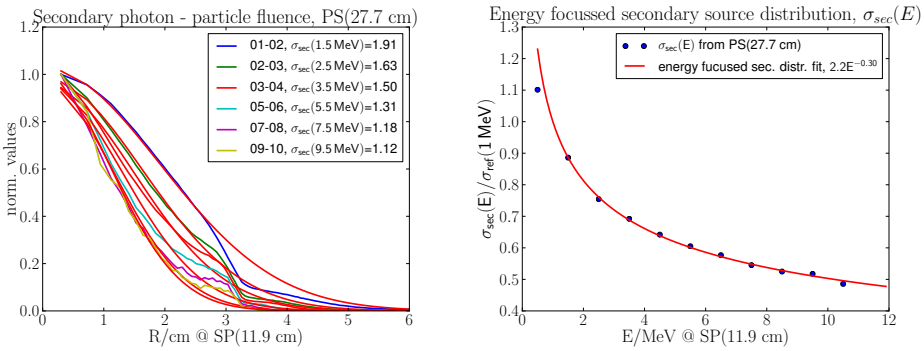

Figure 4.5: Left: The 6MV energy-focussed distribution of the secondary source with the Gaussian fit of its particle fluence calculated in the energy bin. Right: the fit of $\sigma_{sec}(E)$.

The secondary source is described by a Gaussian distribution:

$$\Sigma_{sec}(\sigma_{sec}(E),r) = \frac{1}{2\sqrt{\pi}} e^{-\frac{r^2}{2\sigma^2_{sec}(E)}}, \tag{4.3}$$

where $\sigma_{sec}(E)$ is the secondary source size as a function of particle energy, and r is the distance from the central axis for the position of the particle in the source plane. The BEAMnrc PS(27.7 cm) data, reconstructed at the source plane position, SP(11.9 cm), was used to calculate the particle distributions in discrete 1 MeV energy bins. The particle distribution in each energy bin was fitted with a Gaussian distribution (Equation 4.3) to find $\sigma_{sec}(E)$ for each energy. Only the central part of the secondary particle distributions, R<2.4 cm, were fitted in order to avoid fitting errors due to a complex shape of the BEAMnrc particle profiles outward R>2.4 cm. The R=$\frac{20}{100}$11.9 cm= 2.4 cm corresponds to the projected radius of the maximum field edge to the SP(11.9). Then, the relative change in $\sigma_{sec}(E)$ with respect to the kinetic energy E of the secondary photon was fitted with a power law function:

$$\sigma_{sec}(E) = \begin{cases} \sigma_{ref}\left(\frac{0.511\text{ MeV}}{E_o}\right)^{-k} & ,E < 0.511\text{ MeV}, E_o = 1\text{ MeV} \\ \sigma_{ref}\left(\frac{E}{E_o}\right)^{-k} & ,E \geq 0.511\text{ MeV}, E_o = 1\text{ MeV} \end{cases} \tag{4.4}$$

where σ_{ref} was defined for E=1 MeV and used as a reference secondary source size in the VSM., Both the exponent k and σ_{ref} are dependent on the nominal beam energy (6/15 MV), withσ_{ref} being 2.7 cm and 2.2 cm for the 6 MV and the 15 MV beam models, respectively. The exponent k of the power-law function is equal to 0.49 and 0.30 for the 6 MV and the 15 MV beam model, respectively. Figure 4.4 shows the fit of σ_{ref} for 6 MV to the secondary photon particle fluence calculated from the BEAM PS(27.7 cm) projected to SP(11.9 cm). The left panel shows the energy-focussed distribution of the secondary source with the Gaussian fit of its particle fluence calculated in the energy bins: from 0 to 1 MeV (line 00-01 in the left plot) up to; from 5 to 6 MeV (line 05-06 in the left plot). The right panel shows the fit of $\sigma_{sec}(E)$ (Equation 4.4) (line in the right plot) performed for the particle fluence in each energy bin (points in the right plot).

Figure 4.5 shows the fit of σ_{ref} for 15 MV to the secondary photon particle fluence calculated from the BEAM PS(27.7 cm) projected to SP(11.9 cm). The left panel shows the

energy-focussed distribution of the secondary source with the Gaussian fit of its particle fluence calculated in the energy bins: from 0 to 1 MeV (line 00-01) up to; from 9 to 10 MeV (line 09-10). The right panel shows the fit of $\sigma_{sec}(E)$ (Equation 4.4) (line) performed for the particle fluence in each energy bin (the points in the plot).

Since the power function (Equation 4.4) goes to infinity when the energy goes to zero, $\sigma_{sec}(E)$ is truncated to $\sigma_{sec}(0.511\text{ MeV})$ for energies below E=0.511 MeV. This prevents the low energy secondary photons from being generated at a location far away from the central axis and makes the secondary photon generation more efficient, since fewer of the particles which are absorbed in the beam modifiers then will be included.

An implementation of the corrections of the energy-focused secondary source as as fallow. After sampling the particle start position from the Gaussian source distribution for the nominal energy 1 MeV and sampling the particle energy according to its direction relative to the beam axis according to $p_{sec}(E)$ (Equation 4.1), the energy-focussed source distribution correction is applied by changing the relative statistical weight of the particle with respect to its kinetic energy and the position r in the source plane:

$$w_{EFoc} = \frac{\Sigma_{sec}(\sigma(E), r)}{\Sigma_{sec}(\sigma_{ref}, r)} \tag{4.5}$$

Chapter 5

The Contamination Electron Beam Component

The contamination electrons, as directly ionizing particles, contribute significantly to the surface dose in a patient irradiated by a photon field. For a high energy photon beam and for large fields, contamination electrons contribute with up to 30% of the surface dose [15, 63]. This also significantly affects the dose at the depth of the dose maximum [58] of the applied beam, and thus, a proper modelling of the electron contamination beam component is therefore an important part of the VSM. The electron contamination model (eVSM), developed by the author of this thesis, is described in detail in Appendix B, and in the following a brief overview of this model is given.

There are various methods applied in order to determine the electron contamination: measurements [42, 43, 69, 40], analytical models [72] and Monte Carlo (MC) simulations [79, 39, 14, 61, 23]. The most accurate method is direct MC simulation, but this is an inefficient method for determination of the electron contamination, due to the fact that most of the electrons are absorbed or scattered away from the beam in the collimators and in the air between the accelerator and the patient. For example, for a 20x20 cm^2 field, one would need to simulate $1.3 \cdot 10^9$ and $5.2 \cdot 10^9$ primary electrons for 6 MV and 15 MV respectively, in order to obtain 10^6 contamination electrons on the surface of the patient.

Thus, a model for the electron contamination was developed [66], namely the eVSM. The eVSM is derived from the BEAM simulations with the 6 MV and 15 MV beam models. Further, it comprises a Gaussian distributed electron source located at the base of the flattening filter. The PS representation was achieved by modelling two phenomena: an energy dependent source diameter and an angular dependent particle fluence. The air scatter of the contamination electrons is approximated by the energetic properties of the eVSM, so that explicit in-air transport is not required for MC simulations of the dose distribution in the patient.

The basic idea of the eVSM is to reconstruct the PS properties of the contamination electrons in different scoring plane locations and thereafter, for validation purposes, compare each of them with the PS properties calculated by the direct MC simulation of the accelerator head. The results are used to evaluate properties of the VSM, such as the electron spectrum (Equation 5.1), the Gaussian energy-dependent particle fluence distribution and the enhancement of the focal spot particle fluence.

The energy spectrum (Figure 5.1) is represented by an exponential function (Equation 5.1) which depends only on one open parameter of the eVSM; the electron mean energy $\langle E_e \rangle$. The $\langle E_e \rangle$ can also be obtained from an empirical relation with the nominal beam energy E_{nom} (Equation 5.3) which is a characteristic beam parameter corresponding to the maximum elec-

tric potential used by a linear accelerator to produce the photon beam, conventionally expressed in MV but here we express it in MeV for a unit convention (Equation 5.3). The rest of the parameters are fixed based on full MC simulations.

$$p_e(E) = \frac{1}{N} e^{-\frac{E}{\langle E_e \rangle}} \quad , E_{cut} < E < E_{max} = 0.9 E_{nom} \tag{5.1}$$

$$N = \int_{E_{cut}}^{E_{max}} dt \; e^{-\frac{t}{\langle E_e \rangle}} \tag{5.2}$$

$$\langle E_e \rangle \approx 0.13 \, E_{nom} + 0.55 \text{ MeV} \tag{5.3}$$

The energy spectrum is defined in the range from E_{cut}, E_{cut}=50 keV, to the maximum contamination electron energy E_{max}, $E_{max} = 0.9 E_{nom}$ MeV, respectively.

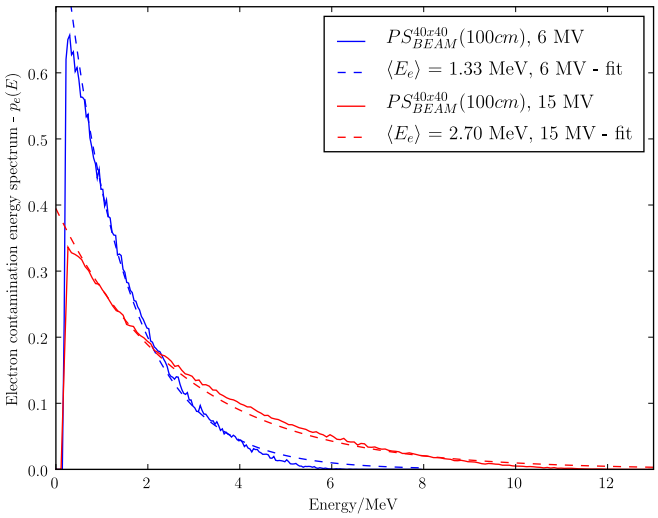

Figure 5.1: The energy spectra of contamination electrons calculated at the isocentre plane (SSD=100cm) from the BEAM PS(100 cm) (solid) and the eVSM $\langle E_e \rangle$ evaluation (dashed) based on Equation 5.3 for 6 MV and 15 MV beams.

The particle fluence of the eVSM, Σ_{eVSM}, at the source plane position, located at the base of the flattening filter, is represented by an energy-focused distribution (Equation 5.4). The source size $\sigma_{econ}(E)$ in Equation 5.5 is energy dependent and as we see, it is described by a power-law function where the exponent k is fitted to the fluence distribution calculated in discrete energy bins (Figure 5.2).

$$\Sigma_{eVSM} = f(\sigma_{econ}(E), r) = \frac{1}{2\sqrt{\pi}} e^{-\frac{r^2}{2\sigma^2_{econ}(E)}} \tag{5.4}$$

$$\sigma_{econ}(E) = \sigma_{ref} \left(\frac{E}{E_0} \right)^k ; k = -0.16, \; E_0 = 1 \text{ MeV} \tag{5.5}$$

One important step in adjusting the eVSM, is the enhancement of the focal spot particle fluence $w_{targ}(r_{targ}, E)$ (Equation 5.6).

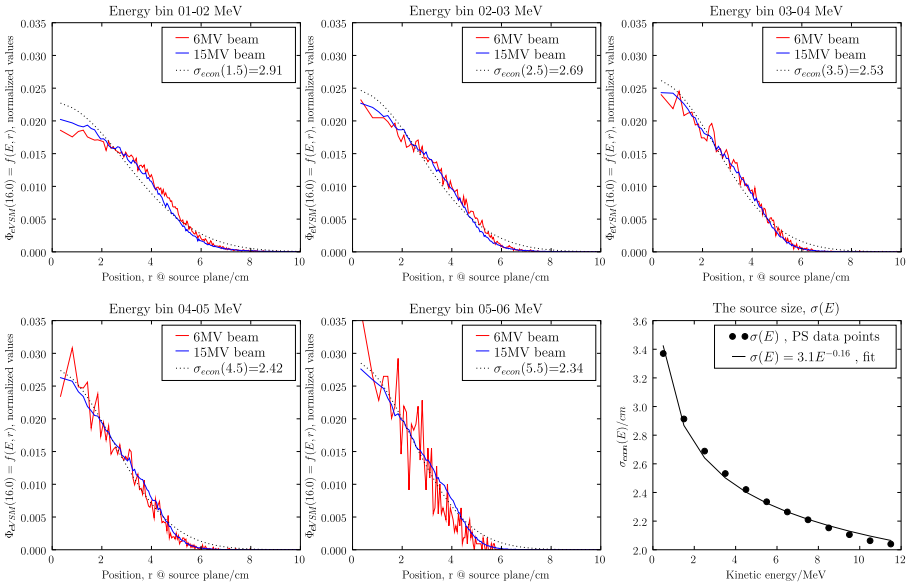

Figure 5.2: Electron fluence distributions calculated at the source plane, SP(16 cm), compared with the corresponding energy bins for 6 MV and 15 MV photon beams. The Gaussian distribution $\Sigma_{\mathrm{eVSM}}(\mathrm{source\,plane})$ is fitted to the BEAM electron fluence PS(source plane) for each energy bin separately. The source size is approximated with a power-law function, $\sigma(E)$ (bottom right).

$$w_{targ}(r_{targ},E) = \frac{\Sigma_{BEAM}(0\text{ cm})}{\Sigma_{eVSM,uncorrected}(0\text{ cm})} \tag{5.6}$$

In Equation 5.6, the particle fluence from the BEAM PS(27.7 cm) projected to SP(0 cm) and the VSM PS(27.7 cm) projected to SP(0 cm) prior to the following correction are denoted as $\Sigma_{BEAM}(0\text{ cm})$ and $\Sigma_{eVSM,uncorrected}(0\text{ cm})$. The $w_{targ}(r_{targ},E)$ represents the change of the statistical weight with respect to the position of the electron in the target plane. A high accuracy of the PS representation in the target plane is crucial for the results when calculating the output factors obtained through the eVSM, since the target point is the geometrical center of the collimation system of the accelerator head.

Electrons, as charged particles, interacts with air and the collimation system as they traverse through the region between the source and the patient. This requires explicit simulation of the contamination electrons from the source to the patient. This would reduce significantely the efficiency of the eVSM. However, It can be avoided by incorporating the previously introduced corrections: the Gaussian energy-dependent particle fluence distribution and the enhancement of the focal spot particle fluence in the eVSM and by using the energy spectrum as it is at the surface of the patient (i.e. at SSD≈100 cm), in contrast to as it is at the source plane location. Although this makes the eVSM less accurate outside the field, it is still acceptable with respect to the total surface dose (Figure 5.4). For more details about the eVSM, it is referred to Appendix B[66].

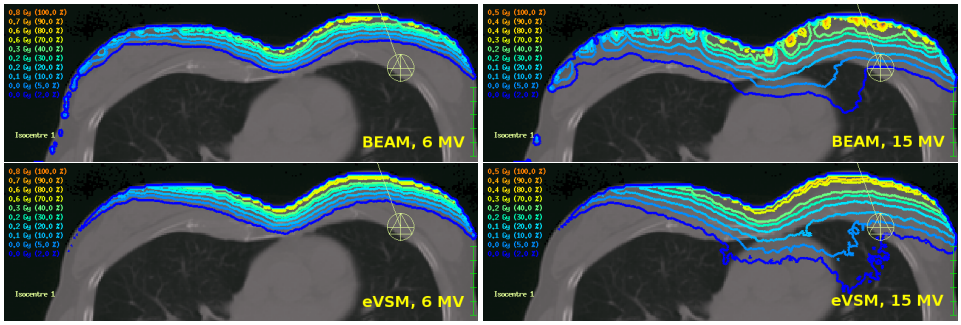

Figure 5.3: The contamination electron dose distributions calculated in a breast case patient geometry for 6 MV (left) and 15 MV (right) photon beams calculated with BEAM (upper) and the eVSM (lower). All plots show the transversal cross section of the breast irradiated with a 20x20 cm^2 field and a gantry angle of 20°. The isodoses are normalized to the maximum dose.

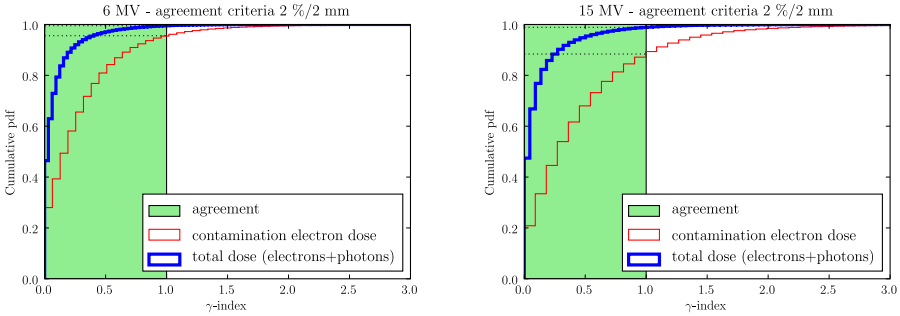

Figure 5.4: The γ index cumulative distributions of the agreement (2%/2 mm) between the 3D dose distributions from the eVSM and the reference BEAM 3D beam models (Figure 5.3).

In Figure 5.3, the contamination electron dose distributions are shown in an example with calculation of dose distribution in a breast patient case. One can see that the eVSM produces a more evenly distributed dose distribution in the surface layers than the dose distributions obtained through full BEAMnrc calculations, both for 6 MV and 15 MV photon beams. As we can see in Appendix B, the BEAM calculation of the contamination electron beam component contains artefacts that do not appear in the eVSM dose distribution.

Figure 5.4shows the γ index cumulative distributions of the agreement (2%/2 mm) between the 3D dose distributions from the eVSM and the reference BEAM 3D beam models (Figure 5.3). When the cumulative probability distribution function (pdf) reaches 1.0 it means that all points of the dose distribution are within the acceptance criteria (2%/2 mm). The blue (thicker) lines illustrate the agreement between 3D electron dose distributions and the red (thinner) lines illustrate the agreement between the total surface dose distribution for 6 MV beam (left) and 15 MV beam (right).

The validation results of the eVSM shows high accuracy when the simulation results were compared with the full MC simulation. This makes it a valuable electron contamination source model for the clinical application. It is due to the eVSM efficiency of particle generation and the simple commissioning routine which requires only a change of the electron mean energy.

Chapter 6

Measurements for Commissioning of the VSM

6.1 The Commissioning Procedure

Through the commissioning procedure of the MC simulation model, the key parameters of the beam model from measurements are obtained. Since all linear accelerators have individual properties, even if they are of the same type or model, they all have to be commissioned separately. It is also a clear advantage that the commissioning procedure is simple and fast. In order to achieve this, a new commissioning method was developed by the author. The method is referred to as the *poly-energetic kernel superposition method*. The poly-energetic kernel superposition method will use (1) direct MC simulation to derive *reference* parameters of the MC beam model for a given type of accelerator, and (2) water measurements to determine *open* parameters of the beam model for an individual accelerator. The reference parameters are characteristic for a given accelerator type and they are determined only once as described in Chapters 3, 4 and 5. The open parameters have to be adjusted for each individual machine separately.

This chapter describes the latter part of commissioning where open parameters of the model are determined based upon comparisons between simulation results and measurements. This part of the work is an important part of the final validation of the VSM in the MC-TPS.

6.2 The Poly-energetic kernel superposition method

The open parameters of the VSM are obtained through fitts, in which the difference between calculated total dose and measured total dose in water is minimized. The total dose, D_{total}, is the superposition of dose components from each radiation source. There are three radiation sources defined in the VSM (Section 2.4.1), therefore D_{total} is calculated as follows:

$$D_{total} = N\{(1-p_{econ})[p_0 D_{pri} + (1-p_0)D_{sec}] + p_{econ}D_{econ}\} \tag{6.1}$$

Where D_{pri}, D_{sec} and D_{econ} are the primary, secondary and electron contamination dose components, respectively. N is the total dose normalization parameter and p_0 and p_{econ} are the relative primary dose contribution and the electron contamination dose contribution to the total dose, respectively.

Together with the two weights p_0 and p_{econ} and the two weights w_0 and w_s, this gives a total of 10 parameters. The fluence warping corrections (Equation 3.8) (h_0 - h_5) are determined separately. The open parameters for each kernel are as follows:

- D_{pri}: σ_0, E_{max}, b_{pri},

- D_{sec}: σ_{sec}, E_{max}, b_{pri},
- D_{econ}: E_{mean}.

The primary (D_{pri}), secondary (D_{sec}) and electron contamination (D_{econ}) kernels are pre-calculated once for each accelerator type and for a small set of values for the open parameters and they are stored for commissioning of individual accelerators. Moreover, D_{pri} and D_{sec} are subdivided in two, a low and a higher, energetic ranges (Equation 6.2 and 6.3). Therefore, two additional kernels $D^{lo}_{pri,sec}$ for the low energy bin ($E_{cut} \leq E < E_{min}$) of the primary and the secondary spectra are required by the commissioning procedure (Equation 6.2 and 6.3). These depend only on the geometrical parameters of the model:

$$D_{pri} = w_0\, D^{lo}_{pri} + (1 - w_0)\, D_{pri}(E_{max}, b_{pri}) \tag{6.2}$$

$$D_{sec} = w_s\, D^{lo}_{sec} + (1 - w_s)\, D_{sec}(E_{max}, b_{sec}) \tag{6.3}$$

Equations 6.2 and 6.3 introduce two new parameters, w_0 and w_s, of the VSM. These parameters represent the relative contribution of the low energy kernel $D^{lo}_{pri,sec}$ and the high energy kernel $D_{pri,sec}$ for the primary and secondary component, respectively.

The poly-energetic kernels are calculated in a virtual water phantom using the XVMC dose engine. For each virtual source, the same amount of particles is generated in order to maintain the same relative dose contributions. The poly-energetic kernel calculation uses all the energetic and geometric parameters of the VSM (Table 6.1). The number of poly-energetic kernels required by the commissioning routine is reduced to a minimum, since most parameters of the VSM are fixed based on analysis of PS information from the full MC simulations in the first step of creating a beam model (Table 6.1). Moreover, the primary photon source size, σ_{pri}, is also fixed to the approximate value of 0.1 cm, during kernel calculations and it is adjusted based upon comparisons with the results from high resolution measurements (Section 6.5) after the determination of the energetic parameters. In case of changes, e.g. accelerator design changes, one would need to investigate the influence of the source sizes (especially σ_{sec} and σ_{econ}) on the commissioned beam model i.e. to calculate additional $D^{lo}_{sec}(\sigma_{sec})$, $D_{sec}(E_{max}, b_{sec}, \sigma_{sec})$ and $D_{econ}(E_{mean}, \sigma_{econ})$ kernels.

When the reference size of the secondary source is fixed based on the BEAMnrc PS data only the energetic variables $E_{max}, b_{pri}, b_{sec}$are open for fitting and the minimum set of poly-energetic kernels contains twenty three kernels calculated for three values of each open parameter, i.e. an initial value, this value + 10%, and this value - 10%, of the initial value which is obtained from an analysis of the PS data:

1. one primary bin kernel: D^{lo}_{pri}, where $E_{cut} \leq E < E_{min}$,
2. nine primary energy-dependent kernels (a variance of two open parameters (E_{max}, b_{pri}) for three values for each parameter: $D_{pri}(E_{max}, b_{pri})$ where $E_{min} \leq E \leq E_{max}$,
3. one secondary bin kernel: D_{sec} where $E_{cut} \leq E < E_{min}$,
4. nine energy-dependent secondary kernels (a variance of two open parameters: (E_{max}, b_{sec}) for three values for each parameter): $D_{sec}(E_{max}, b_{sec})$ where $E_{min} \leq E \leq E_{max}$,
5. three electron contamination kernels (one open parameter): $D_{econ}(E_{mean})$.

Table 6.1: Overview over the fixed and open parameters of the VSM

Parameters	Abbreviation	6 MV	15 MV	Fixed	Open
Primary photon source					
Primary photon contribution	p_0	VSM specific			+
Low energy bin stat. weight	w_o	VSM specific			+
geometric parameters					
Location	Z/cm	0	0	+	
Source diameter	σ_{pri}/cm	0.1076	0.1067		+[†]
Flattening filter	d, r/cm, h	18, 3.65, 0.2d	45, 3.65, 0.2d	+	
Flatness enhancement	$h_{0,\cdots,5}$	VSM specific			+[‡]
energetic parameters					
Energy cut-off	E_{cut}/MeV	0.1	0.1	+	
Bin energy maximum	E_{min}/MeV	0.511	0.511	+	
Maximum energy	E_{max}/MeV	7.7	13.9		+
Spectrum exponent	b_{pri}/MeV^{-1}	1.05	0.76		+
Off-axis energy softening	δb_{pri}/MeV^{-1}	0.62	1.03	+	
Secondary photon source					
Low energy bin stat. weight	w_s	VSM specific			+
geometric parameters					
Location	Z/cm	11.9	11.9	+	
Source diameter	σ_{sec}/cm	2.7	2.2	+	
Source focusing exponent	k	0.49	0.30	+	
energetic parameters					
Energy cut-off	E_{cut}/MeV	as for primary photon source			
Bin energy maximum	E_{min}/MeV	as for primary photon source			
Maximum energy	E_{max}/MeV	as for primary photon source			
Spectrum exponent	b_{sec}/MeV^{-1}	1.17	0.70		+
Off-axis energy softening	δb_{sec}/MeV^{-1}	1.43	1.99	+	
Electron contamination source					
Electron contribution	p_{econ}	VSM specific			+
geometric parameters					
Location	Z/cm	16.0	16.0	+	
Source diameter	σ_{econ}/cm	3.1	3.1	+	
Source focussing exponent	k	0.16	0.16	+	
energetic parameters					
Mean energy	E_{mean}/MeV	1.33	2.5		+
Dose normalization factor	N/Gy/MU	VSM specific			+

[†] - parameter based on high resolution measurements (see Section 6.5)

[‡] - parameters based on lateral large field measurements at a shallow depth (see Section 6.4)

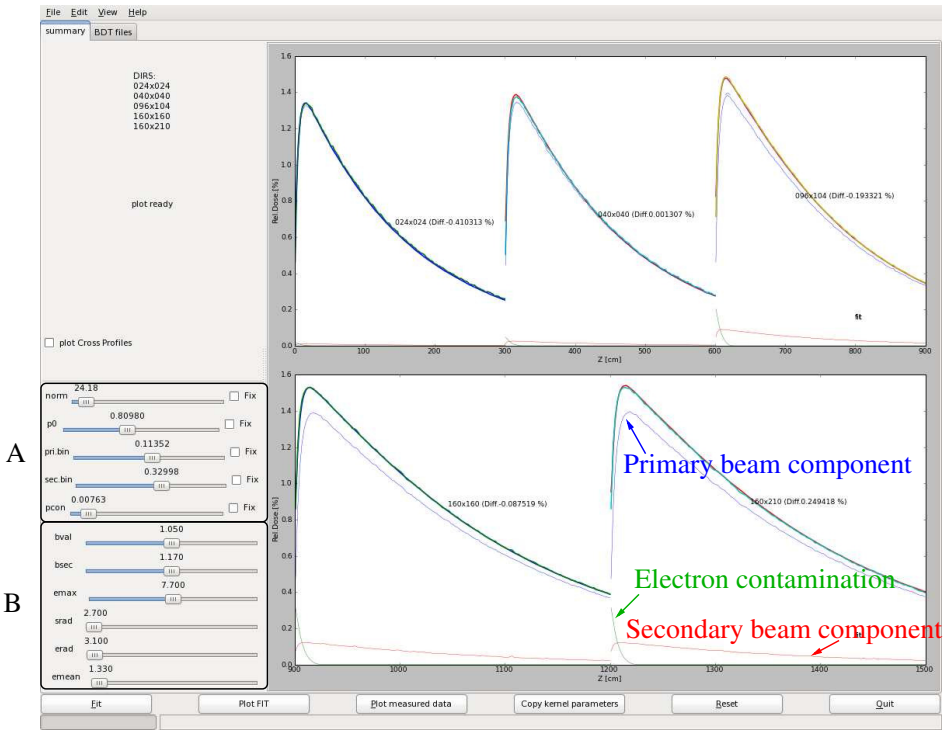

Figure 6.1: The Graphical User Interface (GUI), developed by the author of this thesis, as a commissioning tool; with marked adjustable energetic and (optional) geometrical parameters (A) as well as the relative component contribution parameters (B) of the VSM. Here, an example of a fit of the 6 MV beam model of the Elekta Synergy S linear accelerator is presented for five various field sizes (2.4x2.4, 4x4, 9.6x10.4, 16x16 and 16x21 cm^2). Measured and calculated dose distributions are marked with thick lines while the different beam components are marked with thin lines.

Varying the initial value by $\pm 10\%$ should provide sufficient space over fitting parameters to adjust open parameters for an individual linac.

The Poly-energetic kernels can be calculated for arbitrary values of the open parameters by a linear interpolation of the applied kernels. This task is performed by a commissioning tool developed for this work (Figure 6.1). It composes the total dose from the polyenergetic kernels and thereby fits the open parameters of the VSM. The beam component weights are fitted automatically using a nonlinear Levenberg-Marquardt fitting routine [52] for chosen energetic and geometric parameters of the beam model.

In all models presented in this work all the geometric parameters were fixed based on the full MC simulations. In case of a different accelerator type, a revision of the geometric parameters can be performed by readjusting the geometrical parameters.

Most of the open parameters of the VSM are derived from depth dose curves (which is measured in the z-direction in the linac and measurement coordinate system, hence reffered to as Z-profiles), and the commissioning routine also has to include lateral cross profile data for comparisons between calculations and measurements, especially for large field sizes, this in order to validate the off-axis softening effect or the flattening filter model as well as the fit of the flatness parameters of the model as described below.

6.3 Commissioning data and absolute normalisation

The commissioning data contains a set of measurements performed in order to check the validity of the model in various clinically relevant situations, i.e. measurements for various field sizes, shapes or source to surface distances. The measurement results are used to fit the VSM open parameters and to validate the beam model. The minimal set of measurements includes profiles (depth dose curves and cross profiles) for various field sizes and various depths, all measured in a water phantom with a small size ion chamber. The commissioning measurements used in this work contained: dose profiles measured in water in all directions X,Y and Z for small, reference and large field sizes, with chosen field sizes depending on the MLC type (section 2.5). The cross profiles, X and Y, were measured at the depth of dose maximum 1.5 cm (6 MV) and 2.5 cm (15 MV), the reference depth 10 cm and at the depth of 20 cm in water. Additionally, validation measurements were performed in order to check the commissioned model for various different situations. Those included complex field shapes, heterogeneous density phantoms, fields composed from a number of segments (intensity modulated field), see chapter 7.

Each linear accelerator is calibrated to deliver a defined dose to a reference point under reference conditions. In our clinic, the reference setup is defined such as to deliver a dose of 1 Gy at 10 cm depth in water and SSD=100 cm when irradiating 100 Monitor Units (MU), with the reference field size 10x10 cm^2. The MU is a unit that is proportional with the read out charge from the ionisation chamber in the linear accelerator head. The reference point is important for relative measurements since all read-out from the dosimeter in other points of interest $D(A,z)$ are relative and related to the read-out in the reference point $D(A_{ref},z_{ref})$. The ratio $D(A,z)/D(A_{ref},z_{ref})$ is called an Output Factor (OF) and is defined by Equation 6.4, where A is the field size and z is the depth.

$$OF(A,z) = \frac{D(A,z)}{D(A_{ref},z_{ref})} \tag{6.4}$$

Various dosimetric systems were used to measure dose profiles and dose planes. Dose profiles for large fields were measured in a water phantom with an ion chamber, PTW-31010

(V=0.125 cm^3), while very small fields, smaller than 2x2 cm^2, were measured with a high resolution diamond detector. The dose distribution of irregularly shaped fields required 2D detectors. For this, radiographic films were used in a solid slab phantom made from a water equivalent material. Also, additional measurements were performed with film in a heterogeneous density lung phantom.

6.4 Flatness parameters adjustment

The parameters, $h_{0,\ldots,5}$, are used for correction of the lateral energy fluence (Section 3.2.6) for any deviations from perfectly flat lateral dose profiles. These parameters are derived from the measurement of the largest available cross profile at a shallow depth in water. This is an indirect method, since the absorbed dose in water is not exactly proportional to the primary energy fluence which should be measured in air. There are however several problems with in-air measurements, since the electron contamination has to be shielded. For that, various build-up caps are used to absorb the contamination electrons and to create secondary electron equilibrium. This technique has large measurement uncertainties. The primary energy fluence can be approximated by calculating the ratio between the dose distribution derived through a commissioned VSM for an individual accelerator calculated without flatness correction and the measured dose cross profile for the largest field size at a shallow depth (Figure 6.2). The depth at which this is measured and compared should be a shallow enough depth in order to avoid phantom scatter which will blur the irregularities of the energy fluence. It is recommended to use cross profiles at dose maximum depth which, as we have seen, is 1.5 cm and 2.5 cm for the 6 MV and 15 MV beam models respectively. The ratio between measurement and calculation is taken as a measure of the lateral energy fluence and it is fitted by the enhancement function defined by Equation 3.8.

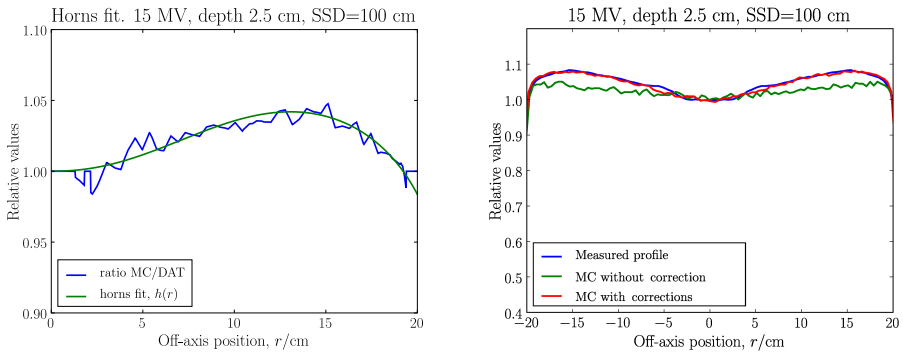

Figure 6.2: Beam flatness adjustment by the ratio between a measured and a calculated (by the polyenergetic kernel superposition) 40x40 cm^2 cross profile measured at 2.5 cm depth in water (left). The effect of dose calculation without and with enhancement of the lateral energy fluence of the same beam (right) can be seen.

The flatness correction function (Equation 3.8) can be fitted in two ways: (1) directly during the commissioning routine by reconstructing the total dose from the separate polyenergetic kernels or, (2) after fitting of the energy spectrum by calculating the total dose with all flatness parameters set to zero. The second method can be useful in case of high statistical noise of the

polyenergetic kernels. Figure 6.2 shows the results of flatness parameter adjustment for the 15 MV Elekta SL*i* accelerator beam model.

6.5 Adjustment of the Size of the Primary Source

A correct evaluation of the primary source size, σ_{pri}, is especially important for small field sizes where the primary source is partially covered by the collimation system. The Output Factors for fields smaller than 2x2 cm^2 drop dramatically due to this shading effect (Figure 6.3). Such small fields are commonly used in stereotactic treatment planning.

The initial estimate of σ_{pri} can be obtained by observing the penumbra width of cross profiles calculated for various primary source sizes and a comparison with the measured cross profile. Linear regression yields an estimate of σ_{pri}.

Commissioning data are as we have said here measured with an ion chamber with a volume of 0.125 cm^3. Since a finite size dosimeter broadens the measured penumbra width, the σ_{pri} delivered from these measurements has a systematic error which can differ more than 30% from the real value [67]. Therefore, high resolution dosimetric systems, like a diamond detector or a diode detector with a very small volume, or alternative methods of deconvolving a finite detector size from measurements [38] have to be used to derive σ_{pri} accurately.

A penumbra based method for evaluation is sufficient for the standard leaf width (1 cm) collimation systems, but for stereotactic applications it is not sufficient. A new method was therefore developed during the work with this thesis (Appendix A) based on the relative change of small field OFs measured with a high resolution detector (diamond detector). Small fields are perfectly suited for primary photon source analysis since only primary photons can pass the collimation system.

The method uses the relative OFs measured for various small field sizes, and calculated OFs for various σ_{pri} values. Since the initial estimate of σ_{pri} is done based on the results from commissioning data measured with ion chamber, σ_{pri} has to be reduced from its initial value. Here, the adjustment of σ_{pri} is presented for the beam modulator with a 0.4 cm leaf width (Figure 6.3).

The advantage of this method is that σ_{pri} adjustment can be performed after fitting all other parameters as a post-commissioning process.

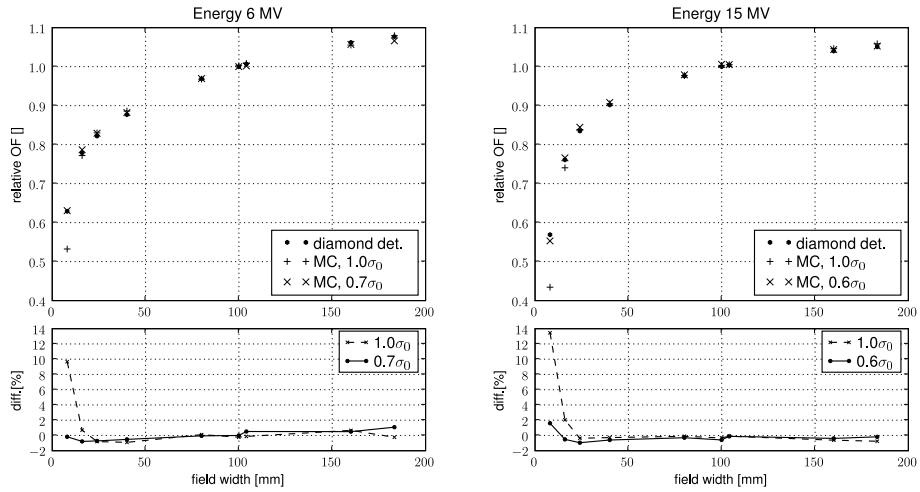

Figure 6.3: The comparison of simulated OF (crosses, stars) and measured OF (bullets) with a diamond detector at 10 cm depth in water (SSD=100 cm) in 6 MV and 15 MV photon beam for field size 9.6x10.4 cm^2. Simulations with the beam model based on the commissioning data measured with an ion chamber V=0.125 cm^3 (crosses) and after readjustment of the primary source diameter (stars).

Chapter 7

Measurement Results and Quality Assurance of the Virtual Source Model

7.1 Small field measurements

The results from small field measurements were used in order to validate the virtual primary photon source properties, since almost only primary particles can pass freely through small fields, due to that these particles or photons originate from the central focal point of the beam, i.e. the central axis in the collimation system. An accurate agreement of depth dose curves (DDCs) and cross profiles (CPs) can be expected to be obtained when the primary spectrum and source size are modelled precisely (Section 6.5).

In the following, results will be shown from measurements, carried out with a diamond detector, showing results from DDCs and CPs of small fields of 0.8x0.8 cm^2 and 1.6x1.6 cm^2 formed by the mini-MLC, all measured in a water phantom. Excellent agreement of all profiles was achieved with the 6 MV and 15 MV VSM data (Figure 7.1). All points agreed better than 2%/2 mm (local difference uncertainty/ distance to agreement) acceptance criteria [5], except at the tail (Z>15 cm) of the 6 MV depth dose curve of 0.8x0.8 cm^2 field where an agreement within 3%/2 mm was found.

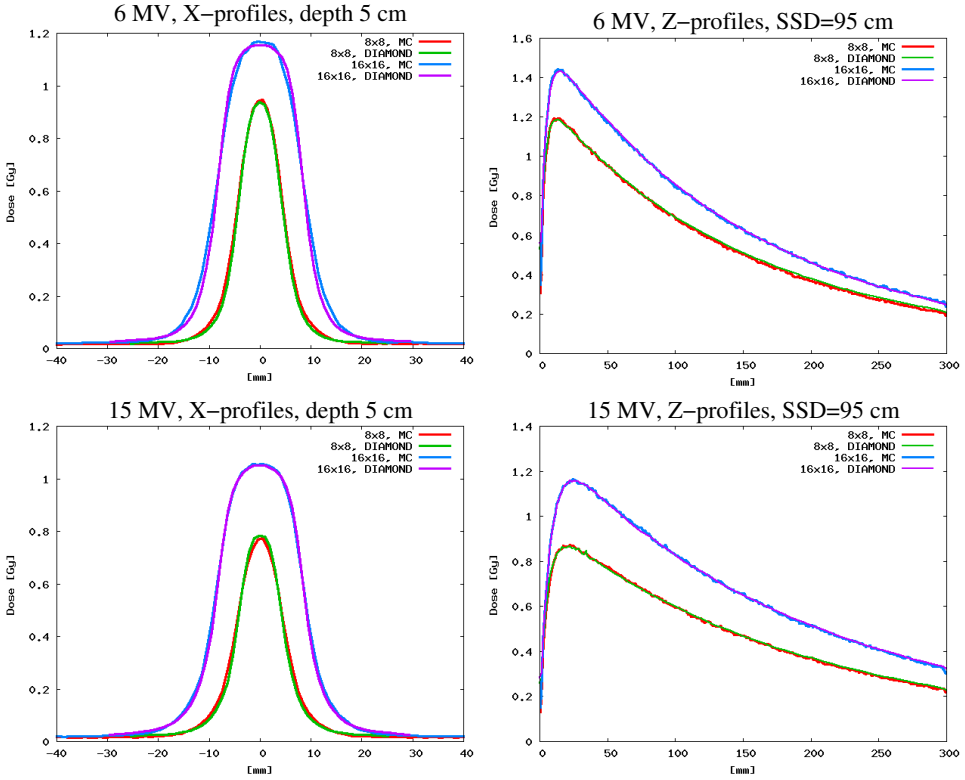

Figure 7.1: Comparison of measured and calculated, with use of the VSM, depth dose (left) and cross profiles at 5 cm depth (right) in water for 0.8x0.8 cm^2 and 1.6x1.6 cm^2 field sizes irradiated with 6 MV (upper) and 15 MV (lower) beam with an Elekta Synergy S linear accelerator. The measurements were performed with diamond detector and a source to surface distance 95 cm.

7.2 Symmetric rectangular fields

As we have already said, all Monte Carlo beam models must be validated with a variety of clinically relevant field sizes. Therefore, the commissioning data include profiles in the X, Y and Z directions (along beam, cross-plane and in-plane) for various field sizes. These data should contain small, reference and large field sizes, and also profiles measured in water at different depths in order to validate the models with respect to accurate reconstruction of all beam components; primary photons (small fields), secondary (large fields) and electron contamination (large fields at shallow depths).

Two types of linear accelerators, the Elekta Precise SLi and the Elekta Synergy S, were commissioned and validated for the energies 6 MV and 15 MV. The Elekta Synergy S linear accelerator was validated for 2.4x2.4, 4x4, 8x8, 10.4x10.4, 16x16 and 16x21 cm^2 field sizes. The Elekta Precise SL*i* linear accelerator was validated for 3x3, 8x8, 10x10, 20x20, 30x30 and 40x40 cm^2 field sizes.

For all profiles, the models showed good agreement between measurements and simulation results, the comparison showed an agreement within 3%/2 mm inside the field and 5%/2 mm outside the field (the tails of cross profiles) (Figures 7.2, 7.3, 7.4, 7.5). The following section shows a selection of small, reference and large field sizes (Figures 7.2, 7.3, 7.4 and 7.5).

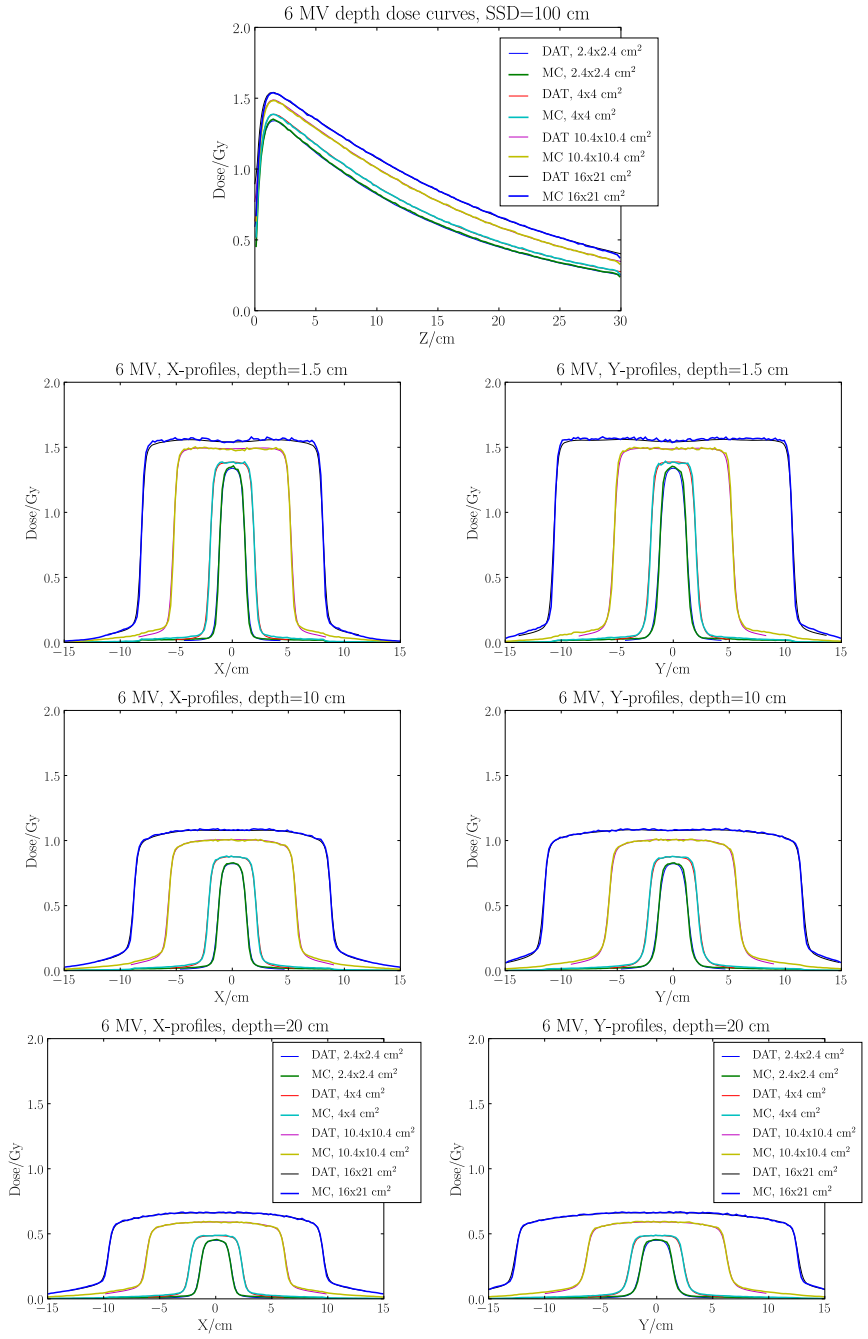

Figure 7.2: Elekta Synergy S. Depth dose profiles (top), X-in-plane (left) and Y-cross-plane (right) profiles measured at 1.5, 10, 20 cm depths in a water phantom located at SSD=100 cm for a 6 MV photon beam compared with MC dose calculations with 2.4x2.4, 4x4, 10.4x10.4 and 16x21 cm^2 field sizes.

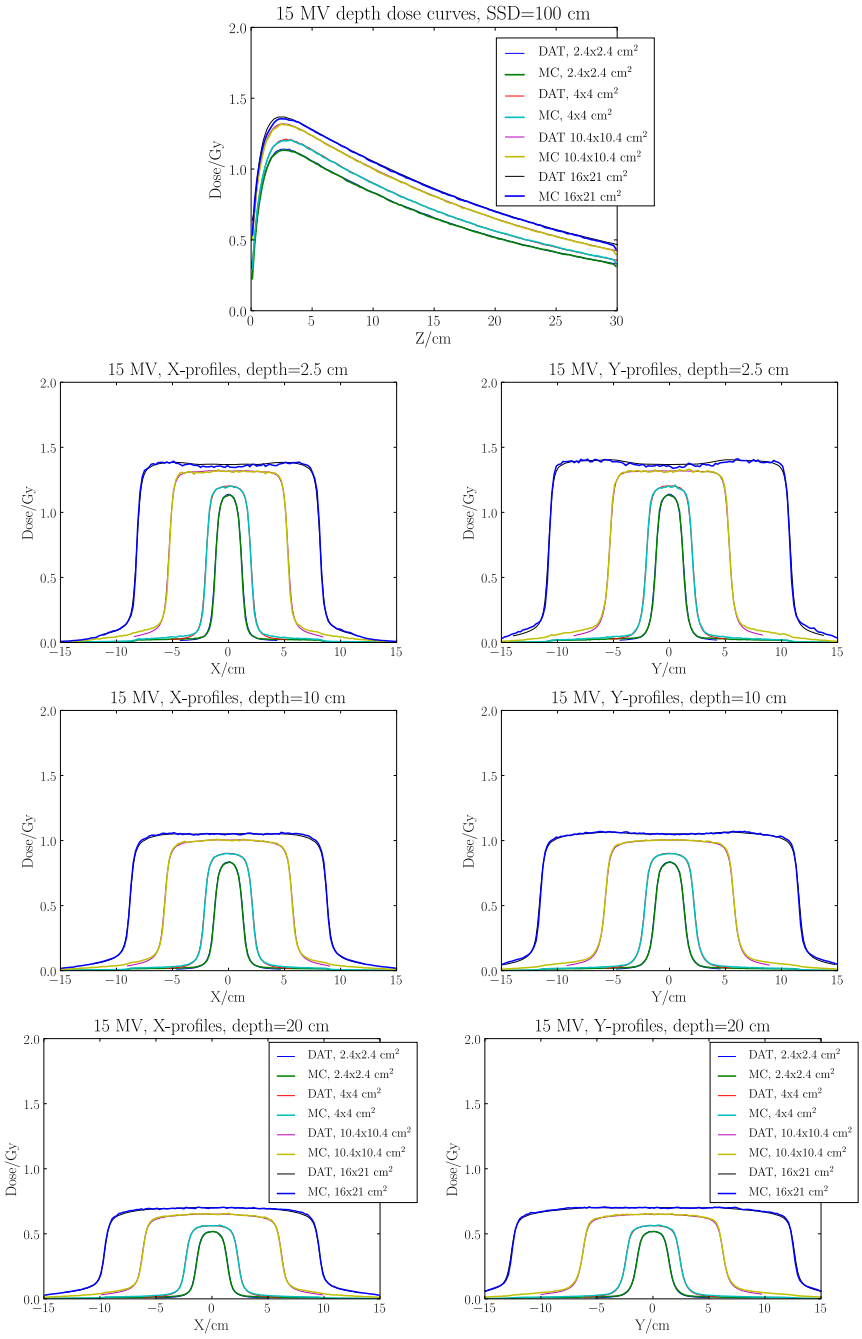

Figure 7.3: Elekta Synergy S. Depth dose profiles (top), X-in-plane (left) and Y-cross-plane (right) profiles measured at 1.5, 10, 20 cm depths in a water phantom located at SSD=100 cm for a 15 MV photon beam compared with MC dose calculations with 2.4x2.4, 4x4, 10.4x10.4 and 16x21 cm^2 field sizes.

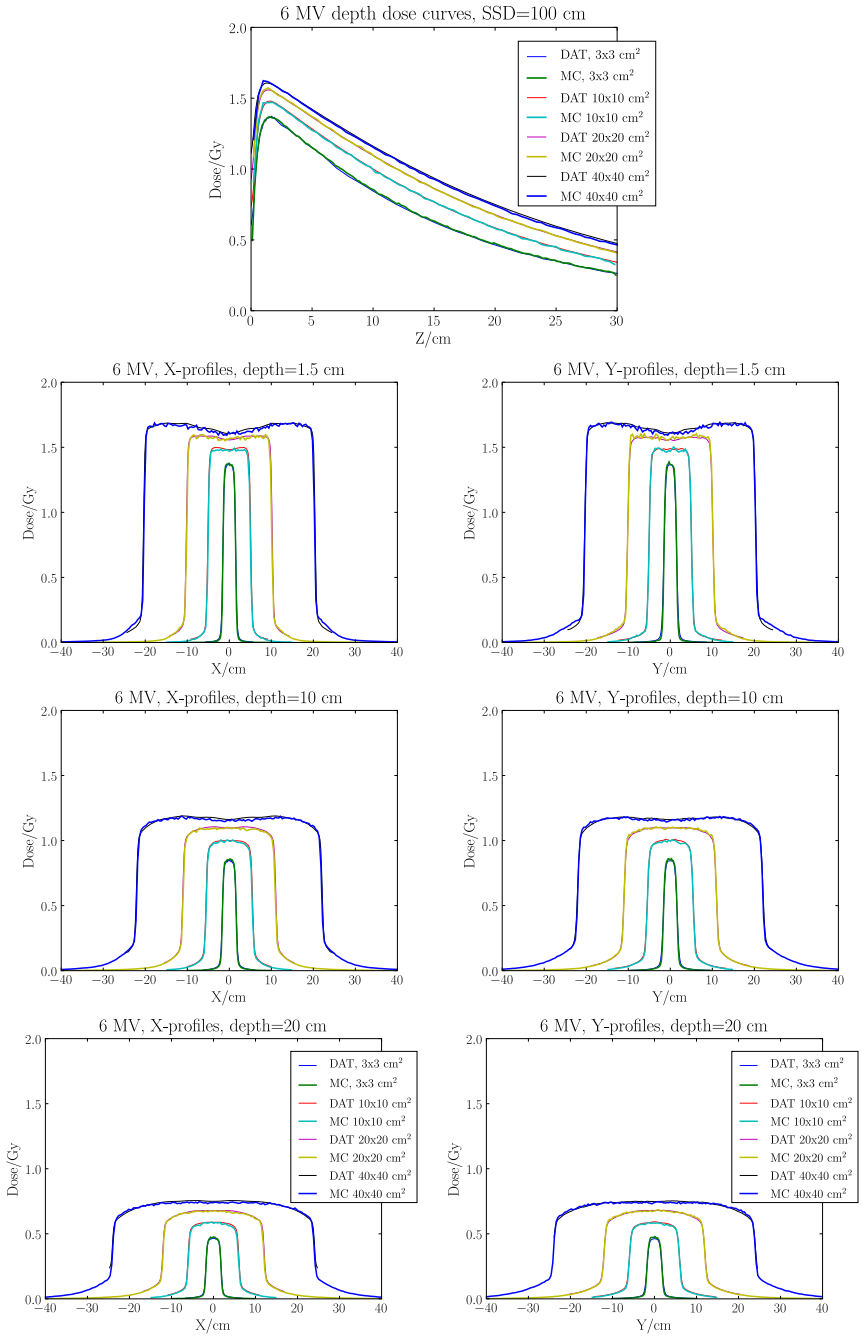

Figure 7.4: Elekta Precise SL*i*. Depth dose profiles (top), X-in-plane (left) and Y-cross-plane (right) profiles measured at 1.5, 10, 20 cm depths in a water phantom located at SSD=100 cm for a 6 MV photon beam compared with MC dose calculations with 3x3, 10x10, 20x20 and 40x40 cm^2 field sizes.

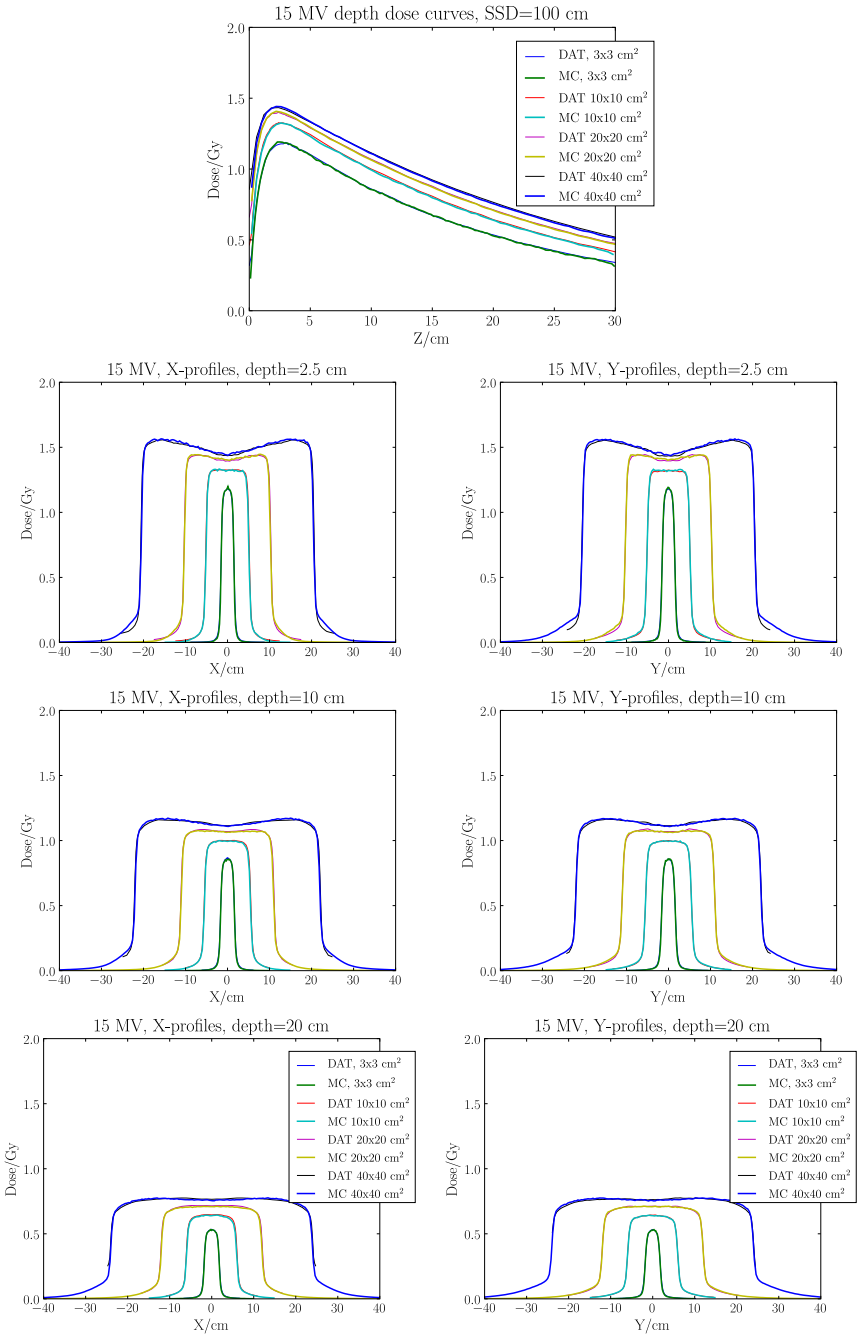

Figure 7.5: Elekta Precise SL*i*. Depth dose profiles (top), X-in-plane (left) and Y-cross-plane (right) profiles measured at 1.5, 10, 20 cm depths in a water phantom located at SSD=100 cm for a 15 MV photon beam compared with MC dose calculations with 3x3, 10x10, 20x20 and 40x40 cm^2 field sizes.

7.3 Highly modulated large fields

As any treatment planning system, also the virtual source model will have to deal with complex intensity modulated (IMRT) beams which are composed of several smaller, complex, MLC shaped field segments. In order to validate the VSM for IMRT fields, several measurements with film dosimetry were performed as a part of the quality assurance (QA) routine at the University Clinic in Tübingen.

All measurements were within the acceptance criteria 3%/2 mm inside the field (high dose regions) and 5%/2 mm outside of the field (low dose regions with $\leq$5% of the dose maximum) compared to the simulation results. The looser constraint for the low dose region is justified by the higher local dose uncertainty of the measurements [76].

An example of the excellent agreement between MC simulations and film measurements are presented in [67] for the Elekta Synergy S linear accelerator. Here, in this work, another example of highly modulated IMRT field measurements of a whole abdomen treatment of a child is given. This is a very complex case where a large irradiation area contains small off-axis segments as well as large segments. A very good agreement (2%/2 mm in the high dose regions and 5%/ 2mm in the low dose region) was achieved, this demonstrates the high accuracy of the VSM for quite sophisticated IMRT plans.

The MC Treatment Planning System HYPERION was used for IMRT treatment planning. This program uses two stages of treatment plan optimisation: i) the Pencil Beam stage and ii) the Monte Carlo stage. The PB stage uses a finite size Pencil Beam (fsPB) algorithm [28] with 3D density corrections [29] implemented. The MC stage uses the XVMC MC dose engine. The PB stage optimises the plan with the beam settings (MLC settings and segment weights) in a conventional way using a so-called beamlets optimisation. Then, the MC stage uses the beam settings obtained in the PB stage for the segment based optimisation where new segment weights are calculated but also new segments are generated. The MC stage is repeated until the treatment plan has converged.

It is possible to use an additional tool, MC verify, provided together with the Hyperion TPS which can be used for a recalculation of already optimized plans. The recalculation can be done on the patient geometry or on arbitrary virtual phantoms both with the PB dose engine and the MC dose engine. Here, we use it for recalculation of IMRT treatment plans with the XVMC dose engine used for dose calculation in the homogenous water phantom in order to compare these with film measurements in a solid water phantom. The IMRT plans were evaluated with PTW-VeriSoft 2.11 (PTW-Freiburg) software. The plans were evaluated qualitatively by comparison of 2D dose distributions calculated at various depths (3 cm and 10 cm) and quantitatively by plotting the γ-factor comparison.

Here, we present one representative comparison of the 2D dose distributions calculated with the XVMC dose engine and measured with the radiographic film at the 3 cm depth in a water phantom for the 15MV IMRT plan delivered by the Elekta SLi linear accelerator. Similar agreement was achieved for another IMRT treatment plans verification for 6 MV and 15 MV beam models of the Elekta SLi and Elekta Synergy S linear accelerators.

7.4 Transmission filter validation

The MLC leaves mounted on the Elekta Precise SL*i* linear accelerator have either a Tongue&Groove (T&G) design [13, 80] or they are rotated away from the primary electron beam focus, as it is done on the Elekta Synergy S linear accelerator, to prevent radiation leakage between them. This produces patterns of under-dosage for adjacent fields if their bound-

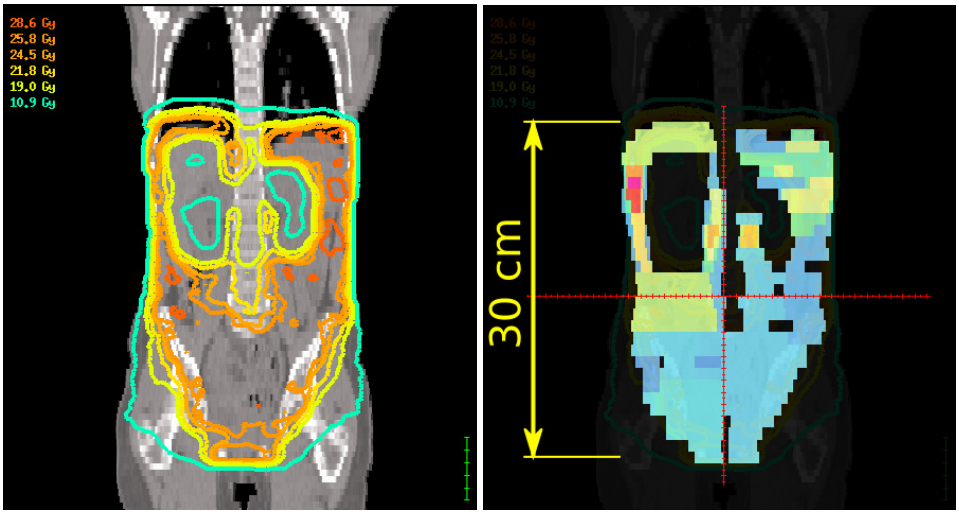

Figure 7.6: The coronal view of an abdomen irradiation of a 4 year old child. Left, the 15 MV dose distribution overlaid on the patient geometry presented as isolines. Right, the highly modulated IMRT beam presented as the fluence map. The beam is created with 25 segments.

aries are formed by the leaves. This is due to a different amount of radiation passing through the variable leaf thickness at the field edge.

In order to validate the transmission filter model for the T&G effect, we have investigated dose distributions obtained through irradiation with nine adjacent fields (Figure 7.9) of 6 MV and 15 MV beams, delivered by the Elekta Synergy S linear accelerator. The fields are organised in a 3x3 grid where fields 1 to 6 have the same size of 3.2x3.2 cm^2 and fields 7 to 9 have 3.2x4.0 cm^2 field size. This arrangement is intended to reveal the T&G effect. There are lower and higher doses delivered along the adjacent field edges as a consequence of the tilted leaf side overlaps. Increased transmission through the curved leaf tip is also present. An increased dose can be found also at the field edge, Y=10.5 cm, under the leaf tips in parked position (Figure 7.10).

Dose distributions were measured at the depth 5 cm with radiographic Kodak X-Omat V film in a solid water phantom located at SSD=95 cm. The total number of monitor units was 50 MU in order to deliver the dose in the sensitive range of the film (< 1.0 Gy). Excellent agreement of 2%/2 mm in the high dose regions and 5%/2 mm in the low dose regions (< 5% of D_{max}) was achieved. This confirms the high accuracy of the VSM as well as it validates the modelling of the beam modifiers by the transmission filter.

7.5 Stereotactic fields in a lung phantom

In the regions of the body with low density (lung, air), MC dose calculations has been shown to be more accurate than conventional algorithms [24]. Especially for small stereotactic fields, the calculation is performed in the presence of lateral electronic disequilibrium. In order to benchmark overall accuracy of our dose engines for the extreme situation of small fields, calculated in the presence of the lateral electron disequilibrium, we first compare our conventional fsPB algorithm and the XVMC algorithm to measurements in a lung phantom. The lung phan-

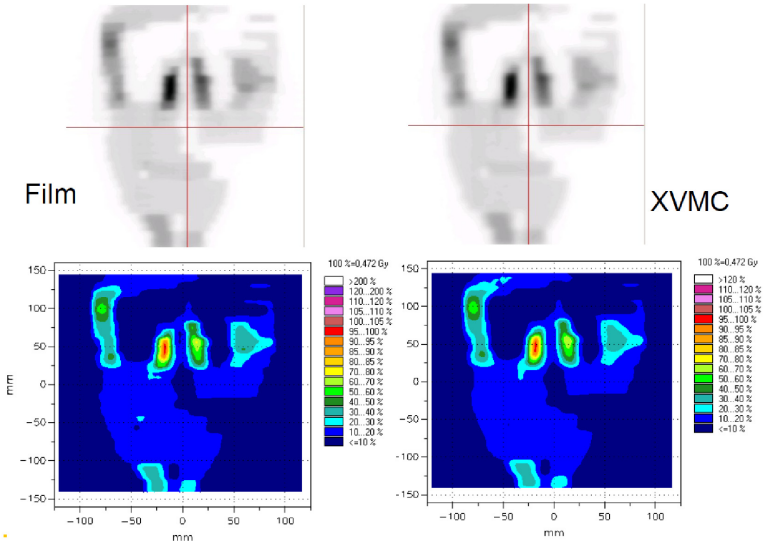

Figure 7.7: Film measurements of a highly modulated 15 MV IMRT beam (the plan applied for the dose distribution seen in Figure 7.6) in a solid water phantom at depth 3 cm (SSD=100 cm) presented as dose planes converted to optical densities (upper) and isodoses (lower). The left column shows measurements while the right column shows MC simulation with XVMC.

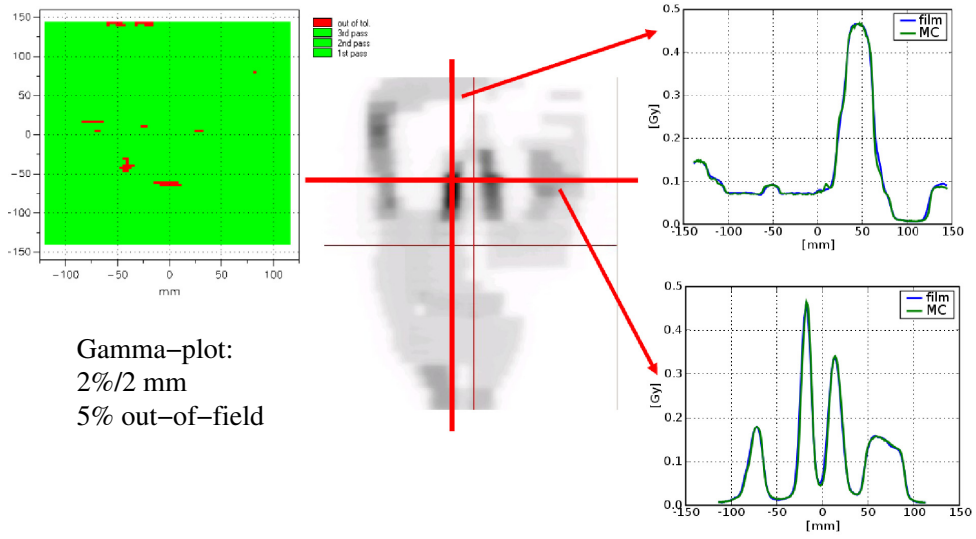

Figure 7.8: Gamma plot and cross profiles of the film verification of the IMRT beam (the plan applied for the dose distribution seen in Figure 7.6), film measurement at 3 cm depth (SSD=100 cm), 15 MV beam energy.

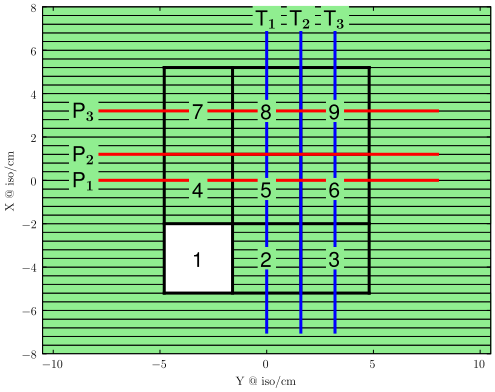

Figure 7.9: The arrangement of nine adjacent fields formed by a Elekta Synergy S linear accelerator with marked parallel profile (P_1, P_2, P_3) and transversal (T_1, T_2, T_3) profiles (right). Fields from 1 to 6 have 3.2x3.2 cm^2 field size and fields from 7 to 9 have 3.2x4 cm^2 field size.

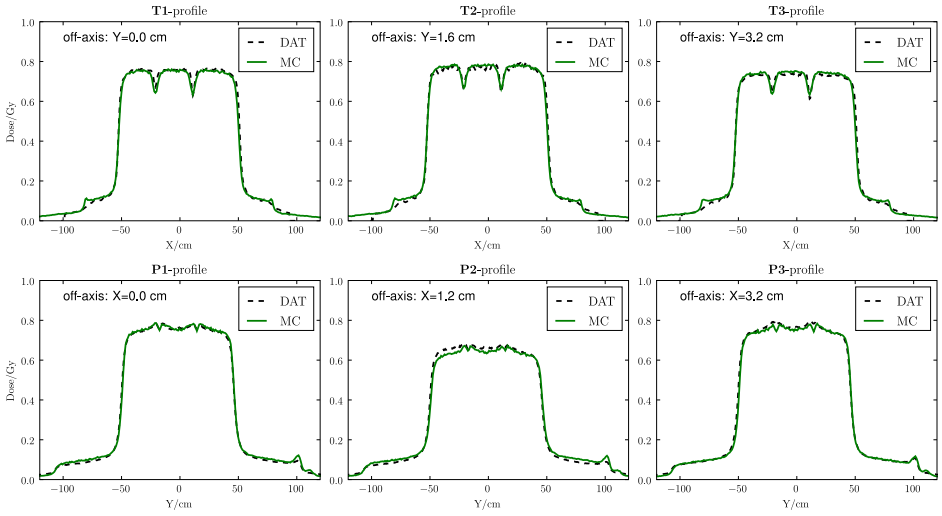

Figure 7.10: The QA dose distribution (T_1, T_2, T_3 and P_1, P_2, P_3 profiles) of the Elekta Synergy S Beam Modulator (BM) created by nine adjacent fields (Figure 7.9, right) measured with a film (DAT - dashed lines) in the solid phantom (SSD=95 cm, depth 5 cm) and MC calculations (MC - solid lines).

tom (Figure 7.11) modelled a small tumour surrounded by lung tissue. Three plastic spheres representing tumours of 2.7, 4.2 and 5.0 cm diameter were used. For each tumour size, a conformal plan consisting of one vertical beam was created using 6 MV and 15 MV nominal beam energies, and the dose delivered to the phantom was calculated both with XVMC and the fsPB. For the MC dose calculation the photon beam was modelled by the VSM. Here, we present the γ comparison of the dose calculation with both algorithms and film measurements in a lung phantom for all tumour sizes (Figure 7.11). Overall, a good agreement was found between MC dose calculation and film measurements, with more than 97% of the points fulfilling the 3%/3 mm acceptance criteria. For the fsPB algorithm the agreement was worse both inside and outside the tumour, 45-81% of all point fulfilled the 3%/3 mm acceptance criteria (Figure 7.12). Appendix C [68] shows more results of the dose calculation performed by these dose engines in the lung phantom where uncertainties of the fsPB up to 8% in the target region and up to 20 % in the region outside of the target have been shown.

These results confirm that MC dose calculations with the use of the VSM perform better than the conventional algorithm, like the fsPB, for stereotactic treatment planning.

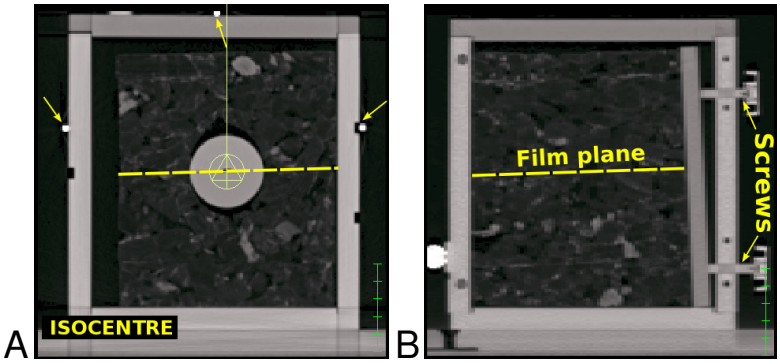

Figure 7.11: Cross sections through the CT scan of the lung phantom which consisted of a low density cork cube surrounding a homogeneous plastic sphere of variable diameter (here: 4.2 cm). The cork cube densities ranged from $\rho_{min} = 0.001$ to $\rho_{max} = 1.09 \frac{g}{cm^3}$ with an average density of $\rho_{mean} = 0.12 \frac{g}{cm^3}$, while the plastic sphere had a density of $\rho = 1.1 \frac{g}{cm^3}$. A film could be positioned through the phantom as marked with a dashed line in A and B. The cork cube, plastic sphere and film were fixed relative to the high density positioning markers (indicated by arrows on A) on the surface of the plastic container by a plastic plate and four plastic screws as shown in B.

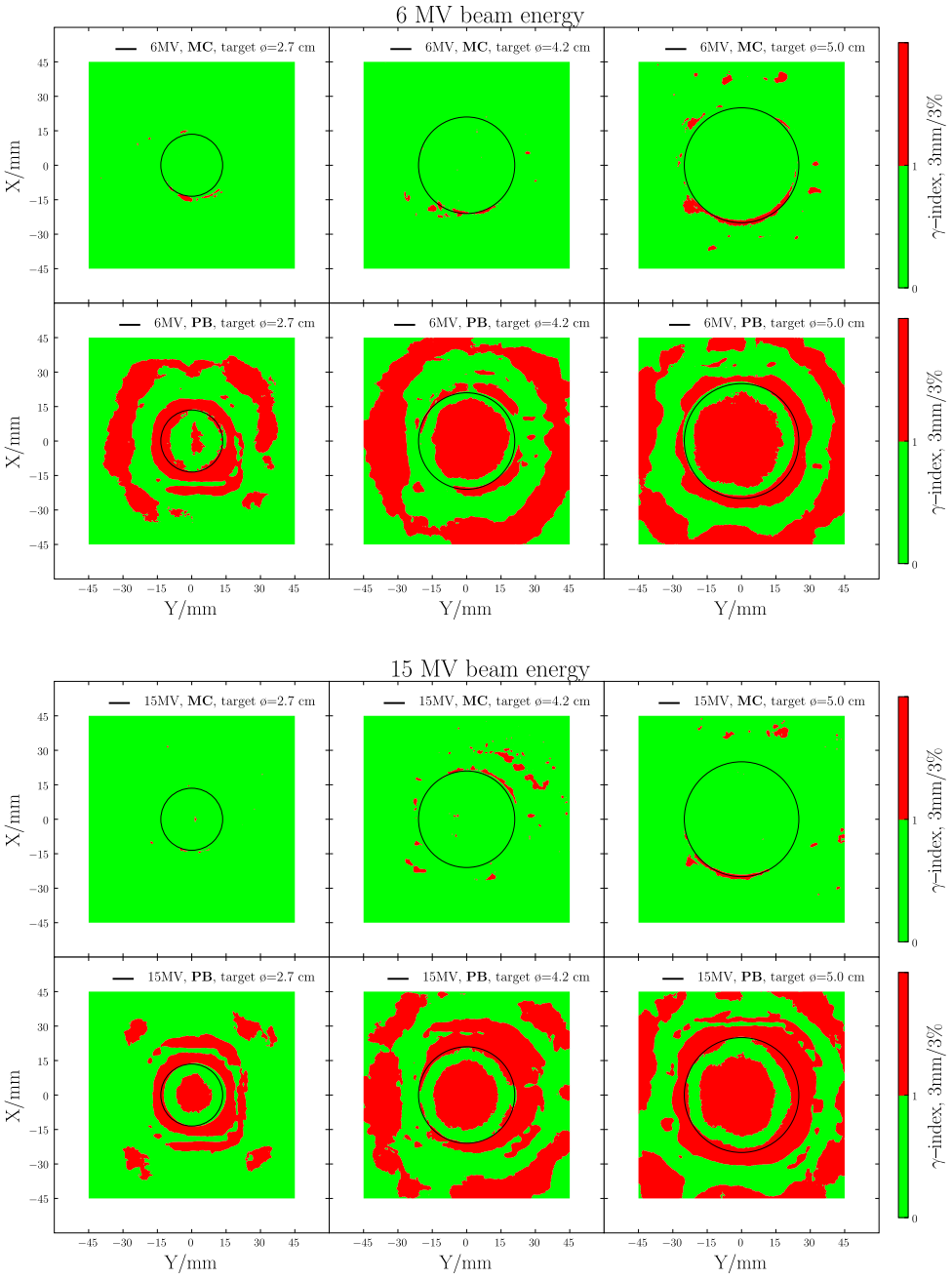

Figure 7.12: A set of γ-plots of the dose distributions measured with film and calculated with MC and fsPB for all tumour sizes for 6 MV (upper set) and 15 MV (lower set). The acceptance criteria for the γ comparisons was set to 3%/3 mm. The tumour outlines are marked by black circles.

Chapter 8

Summary & Conclusion

This thesis has had as aim to describe the implementation and development of a Virtual Source Model (VSM) of clinical photon beams for use in a Monte Carlo treatment planning system (MC-TPS).

In this chapter, a summary of the basic ideas behind our VSM and its commissioning routine including the results of the comparison of measurements and simulations is given.

The key concepts and features of the VSM are discussed in more detail in Appendix A and Appendix B. Appendix A presents improvements to the existing VEF model [21] which is commissioned based on an extensive set of measurements in air and in water and which is different from the VSM model presented in this thesis. Still, the concept of the differential effect of the flattening filter on the primary photon spectrum and the modelling stays the same. Further, improvements of the VSM were done based on the analysis of the Phase Space data simulated with BEAMnrc simulations. This made it possible to eliminate a large source of uncertainties - the air measurements from the commissioning routine. Appendix B shows a new source of contamination electrons as it is implemented in the VSM. The high accuracy of the VSM is confirmed in the work presented in Appendix C, where the results of the stereotactic treatment planning and model validation in the presence of the lateral electronic disequilibrium are presented.

The VSM developed in this thesis work comprises three virtual Gaussian sources, that in turn are representing three main therapeutic photon beam components: i) the primary photon source, ii) the secondary photon source and iii) the electron contamination source. They are located at; i) the target position, ii) the base of the primary collimator and iii) at the base of the flattening filter, respectively. The virtual sources are defined by analytical functions of reference parameters and open parameters. The reference parameters are derived from full MC simulations of the geometrical model of the accelerator head and the open parameters are derived from a fit based upon a comparison between simulation results and measurements.

The basic idea of this project was to develop a beam model for a clinical broad photon beam. The model should be complex enough to meet the highest demands on dose calculation for new techniques used in radiotherapy like lung SBRT (Appendix C). At the same time it should be simple enough to ensure a stable and robust commissioning routine. This was achieved by combining the following ideas:

1. identifying the nature of beam components by a Phase Space (PS) analysis,
2. identifying models and reference parameters which are universal,
3. defining a few open parameters that need to be tuned by comparisons with measurements,

4. developing a robust commissioning method by poly-energetic kernels,

5. performing simultaneous validation of the VSM during commissioning.

By using full MC simulations of the accelerator head, we obtained all information that is necessary in order to identify radiation sources for the VSM by a Phase Space analysis. This would be very difficult or even impossible to achieve for a clinical accelerator by empirical methods. For example, there is no other method other than Monte Carlo simulations suited to analyse electron contamination fluence distributions in energy bins as well as to derive the properties of the energy-dependent secondary source. Further, in situations where direct measurements are very difficult, or even impossible, due to very small fields, steep dose gradients, heterogeneous geometry or inaccessible volumes for dosimeters, a well commissioned geometrical head model simulated with a full MC algorithm can be considered as reference. Therefore it is recommended to use Phase Space information from full Monte Carlo simulations to define the radiation sources, as it has been done in this work.

In order to identify the universal reference parameters of the VSM which are fixed during commissioning, we used full MC simulations. Although this procedure relies on the cumbersome commissioning of the full MC accelerator head model, the commissioning has to be done only once for a given type of accelerators. The open parameters of the VSM are determined by using relevant commissioning data for an individual accelerator. The commissioning is based solely on water measurements which are easily provided by standard dosimetric equipment and routines.

The previous beam model [21] had to be commissioned by an extensive set of measurements in air which was performed with a build-cap on top of the ionization chamber in order to eliminate contamination electrons. This introduces systematic errors into the commissioning data which translates into an inaccurate beam model. In order to eliminate in-air measurements from the commissioning routine, the poly-energetic kernel superposition method of the VSM commissioning was developed. This method is robust due to a small amount of open parameters to be fitted and it is fast since it uses already precomputed poly-energetic kernels.

Moreover, the validation of the VSM occurs simultaneous with the commissioning because the latter is designed such that only one unique set of open parameters generates all the commissioning measurements.

The high accuracy of the VSM was shown for standard rectangular fields as well as for complex IMRT fields, for low energy beams, 6 MV, as well as for high energy beams, 15 MV, for two types of accelerators. Also, the dose distribution when applying very small fields were investigated in water and in a heterogeneous lung phantom. All simulation results agreed very well with measurements, showing the high accuracy of the MC VSM system.

In conclusion, a VSM for a clinical broad photon beam was developed which is accurate and efficient. The VSM model overcomes problems related to full MC simulations of the accelerator head like long simulation time, cumbersome commissioning routine and dependency on the technical information about the accelerator head. This Virtual Source Model enables a broad implementation of a Monte Carlo - Treatment Planning System in the clinical routine at a Hospital Radiation Treatment Department.

Bibliography

[1] ALBER, M., BIRKNER, M., LAUB, W., AND NÜSSLIN, F. Hyperion: An integrated IMRT planning tool. In *13th International Conference on the Use of Computers in Radiation Therapy, Heidelberg Germany* (May 2000), Springer-Verlag Berlin Heidelberg New York, pp. 46–48.

[2] ANTOLAK, J. A., BIEDA, M. R., AND HOGSTROM, K. R. Using Monte Carlo methods to commission electron beams: a feasibility study. *Med Phys 29*, 5 (May 2002), 771–86.

[3] ARNFIELD, M. R., SIANTAR, C. H., SIEBERS, J., GARMON, P., COX, L., AND MOHAN, R. The impact of electron transport on the accuracy of computed dose. *Med Phys 27*, 6 (June 2000), 1266–74.

[4] ASPRADAKIS, M. M., MORRISON, R. H., RICHMOND, N. D., AND STEELE, A. Experimental verification of convolution/superposition photon dose calculations for radiotherapy treatment planning. *Phys Med Biol 48*, 17 (Sept. 2003), 2873–93.

[5] BAKAI, A., ALBER, M., AND NÜSSLIN, F. A revision of the gamma-evaluation concept for the comparison of dose distributions. *Phys Med Biol 48*, 21 (Nov. 2003), 3543–53.

[6] BERGER, M. J., AND SELTZER, S. M. ETRAN, Monte Carlo code system for electron and photon transport through extended media. Tech. Rep. RISC computer code package CCC-107, Oak Ridge National Laboratory, Oak Ridge, TN, 1973.

[7] BIELAJEW, A. F., AND ROGERS, D. W. O. PRESTA: The Parameter Reduced Electron-Step Transport Algorithm for electron Monte Carlo transport. . *Nuclear Instruments and Methods* (1987), B18:165–181.

[8] BOYER, A. L., OCHRAN, T. G., NYERICK, C. E., WALDRON, T. J., AND HUNTZINGER, C. J. Clinical dosimetry for implementation of a multileaf collimator. *Med Phys 19*, 5 (1992), 1255–61.

[9] BRIESMEISTER, J. F. MCNP - A general Monte Carlo N-Particle Transport Code, Version 4C. Tech. rep., Technical Report No LA-13709-M Los Alamos National Laboratory, 2000.

[10] CARRASCO, P., JORNET, N., DUCH, M. A., WEBER, L., GINJAUME, M., EUDALDO, T., JURADO, D., RUIZ, A., AND RIBAS, M. Comparison of dose calculation algorithms in phantoms with lung equivalent heterogeneities under conditions of lateral electronic disequilibrium. *Med Phys 31*, 10 (Oct. 2004), 2899–911.

[11] CHEN, Y., BOYER, A. L., AND MA, C. M. Calculation of x-ray transmission through a multileaf collimator. *Med Phys 27*, 8 (Aug. 2000), 1717–26.

[12] CHETTY, I. J., CURRAN, B., CYGLER, J. E., DEMARCO, J. J., EZZELL, G., FADDEGON, B. A., KAWRAKOW, I., KEALL, P. J., LIU, H., MA, C. M. C., ROGERS, D. W. O., SEUNTJENS, J., SHEIKH-BAGHERI, D., AND SIEBERS, J. V. Report of the AAPM Task Group No. 105: Issues associated with clinical implementation of Monte Carlo-based photon and electron external beam treatment planning. *Med Phys 34*, 12 (Dec. 2007), 4818–53.

[13] CHUI, C. S., LOSASSO, T., AND SPIROU, S. Dose calculation for photon beams with intensity modulation generated by dynamic jaw or multileaf collimations. *Med Phys 21*, 8 (Aug. 1994), 1237–44.

[14] DENG, J., JIANG, S. B., KAPUR, A., LI, J., PAWLICKI, T., AND MA, C.-M. Photon beam characterization and modelling for Monte Carlo treatment planning. *Physics in Medicine and Biology 45*, 2 (2000), 411–427.

[15] DING, G. X. Energy spectra, angular spread, fluence profiles and dose distributions of 6 and 18 mv photon beams: results of monte carlo simulations for a varian 2100ex accelerator. *Phys Med Biol 47*, 7 (Apr. 2002), 1025–46.

[16] DING, W., JOHNSTON, P. N., WONG, T. P. Y., AND BUBB, I. F. Investigation of photon beam models in heterogeneous media of modern radiotherapy. *Australas Phys Eng Sci Med 27*, 2 (June 2004), 39–48.

[17] DOBLER, B., WALTER, C., KNOPF, A., FABRI, D., LOESCHEL, R., POLEDNIK, M., SCHNEIDER, F., WENZ, F., AND LOHR, F. Optimization of extracranial stereotactic radiation therapy of small lung lesions using accurate dose calculation algorithms. *Radiat Oncol 1* (2006), 45.

[18] DOHM, O. S. *Monte-Carlo simulation of small field dosimetry in radiotherapy with high-energy photons*. PhD thesis, Eberhard Karls Universität Tübingen, 2005.

[19] FASSO, A., FERRARI, A., AND SALA, P. R. Electron-photon transport in FLUKA: Status. In *Proceedings of the Monte Carlo 2000 Conference,* (2000), pp. 159–164.

[20] FIPPEL, M. Fast monte carlo dose calculation for photon beams based on the vmc electron algorithm. *Med Phys 26*, 8 (Aug. 1999), 1466–75.

[21] FIPPEL, M., HARYANTO, F., DOHM, O., NÜSSLIN, F., AND KRIESEN, S. A virtual photon energy fluence model for monte carlo dose calculation. *Med Phys 30*, 3 (Mar 2003), 301–311.

[22] FIPPEL, M., AND NÜSSLIN, F. Smoothing monte carlo calculated dose distributions by iterative reduction of noise. *Phys Med Biol 48*, 10 (May 2003), 1289–1304.

[23] FIX, M. K., STAMPANONI, M., MANSER, P., BORN, E. J., MINI, R., AND RÜEGSEGGER, P. A multiple source model for 6 mv photon beam dose calculations using monte carlo. *Phys Med Biol 46*, 5 (May 2001), 1407–1427.

[24] FRAASS, B. A., SMATHERS, J., AND DEYE, J. Summary and recommendations of a National Cancer Institute workshop on issues limiting the clinical use of Monte Carlo dose calculation algorithms for megavoltage external beam radiation therapy. *Med Phys 30*, 12 (Dec. 2003), 3206–16.

[25] GIANNI, S., RAVNDAL, S., AND M., M. *GEANT - Detector Description and Simulation Tool*. CERN - European Organisation for Nuclear Research, October 1994.

[26] HUQ, M. S., DAS, I. J., STEINBERG, T., AND GALVIN, J. M. A dosimetric comparison of various multileaf collimators. *Phys Med Biol 47*, 12 (June 2002), N159–70.

[27] HUQ, M. S., YU, Y., CHEN, Z. P., AND SUNTHARALINGAM, N. Dosimetric characteristics of a commercial multileaf collimator. *Med Phys 22*, 2 (Feb. 1995), 241–7.

[28] JELEŃ, U., AND ALBER, M. A finite size pencil beam algorithm for IMRT dose optimization: density corrections. *Phys Med Biol 52*, 3 (Feb. 2007), 617–33.

[29] JELEŃ, U., SÖHN, M., AND ALBER, M. A finite size pencil beam for IMRT dose optimization. *Phys Med Biol 50*, 8 (Apr. 2005), 1747–66.

[30] JORDAN, T. J., AND WILLIAMS, P. C. The design and performance characteristics of a multileaf collimator. *Phys Med Biol 39*, 2 (Feb. 1994), 231–51.

[31] KAWRAKOW, I. Accurate condensed history Monte Carlo simulation of electron transport. I. EGSnrc, the new EGS4 version. *Medical Physics 27*, 3 (2000), 485–498.

[32] KAWRAKOW, I. VMC++, electron and photon Monte Carlo calculations optimized for Radiation Treatment Planning. *Advanced Monte Carlo for Radiation Physics, Particle Transport Simulation and Applications: Proc. Monte Carlo 2000 Meeting (Lisbon)* (2000), 229–36.

[33] KAWRAKOW, I., AND FIPPEL, M. Investigation of variance reduction techniques for monte carlo photon dose calculation using xvmc. *Phys Med Biol 45*, 8 (Aug 2000), 2163–2183.

[34] KAWRAKOW, I., FIPPEL, M., AND FRIEDRICH, K. 3D electron dose calculation using a Voxel based Monte Carlo algorithm (VMC). *Med Phys 23*, 4 (Apr. 1996), 445–57.

[35] KEALL, P. J., SIEBERS, J. V., ARNFIELD, M., KIM, J. O., AND MOHAN, R. Monte Carlo dose calculations for dynamic IMRT treatments. *Physics in Medicine and Biology 46*, 4 (2001), 929–941.

[36] KRIEGER, T., AND SAUER, O. A. Monte carlo- versus pencil-beam-/collapsed-cone-dose calculation in a heterogeneous multi-layer phantom. *Phys Med Biol 50*, 5 (Mar. 2005), 859–68.

[37] LAUB, W., ALBER, M., BIRKNER, M., AND NÜSSLIN, F. Monte Carlo dose computation for IMRT optimization. *Phys Med Biol 45*, 7 (July 2000), 1741–54.

[38] LAUB, W. U., AND WONG, T. The volume effect of detectors in the dosimetry of small fields used in IMRT. *Medical Physics 30*, 3 (2003), 341–347.

[39] LEWIS, R. D., RYDE, S. J., HANCOCK, D. A., AND EVANS, C. J. An mcnp-based model of a linear accelerator x-ray beam. *Phys Med Biol 44*, 5 (May 1999), 1219–30.

[40] LING, C. C., SCHELL, M. C., AND RUSTGI, S. N. Magnetic analysis of the radiation components of a 10 mv photon beam. *Med Phys 9*, 1 (1982), 20–6.

[41] LIU, H. H., MACKIE, T. R., AND MCCULLOUGH, E. C. A dual source photon beam model used in convolution/superposition dose calculations for clinical megavoltage x-ray beams. *Med Phys 24*, 12 (Dec. 1997), 1960–74.

[42] LOPEZ MEDINA, A., TEIJEIRO, A., GARCIA, J., ESPERON, J., TERRON, J. A., RUIZ, D. P., AND CARRION, M. C. Characterization of electron contamination in megavoltage photon beams. *Med Phys 32*, 5 (May 2005), 1281–92.

[43] LOPEZ MEDINA, A., TEIJEIRO, A., SALVADOR, F., MEDAL, D., VAZQUEZ, J., SALGADO, M., AND CARRION, M. C. Comparison between tg-51 and trs-398: electron contamination effect on photon beam-quality specification. *Phys Med Biol 49*, 1 (Jan. 2004), 17–32.

[44] LOSASSO, T., CHUI, C. S., AND LING, C. C. Physical and dosimetric aspects of a multileaf collimation system used in the dynamic mode for implementing intensity modulated radiotherapy. *Med Phys 25*, 10 (Oct. 1998), 1919–27.

[45] MA, C. Characterization of computer simulated radiotherapy beams for Monte-Carlo treatment planning. *Radiation Physics and Chemistry 53*, 3 (1998), 329–344.

[46] MA, C. M., FADDEGON, B. A., ROGERS, D. W., AND MACKIE, T. R. Accurate characterization of monte carlo calculated electron beams for radiotherapy. *Med Phys 24*, 3 (Mar. 1997), 401–16.

[47] MA, C. M., LI, J. S., PAWLICKI, T., JIANG, S. B., AND DENG, J. MCDOSE - a Monte Carlo dose calculation tool for radiation therapy treatment planning. In *In W. Schlegel and T. Bortfeld, editors, The Use of Computers in Radiotherapy, XIIIth Int'l Conf., Heidelberg* (2000), pp. 123–125.

[48] MA, C. M., MOK, E., KAPUR, A., PAWLICKI, T., FINDLEY, D., BRAIN, S., FORSTER, K., AND BOYER, A. L. Clinical implementation of a Monte Carlo treatment planning system. *Med Phys 26*, 10 (Oct. 1999), 2133–43.

[49] MA, C. M., AND ROGERS, D. W. O. Beam characterization: a multiple-source model. Pirs 509d, National Research Council of Canada, Ottawa, Canada, 1995.

[50] MCDERMOTT, P. N., HE, T., AND DEYOUNG, A. Dose calculation accuracy of lung planning with a commercial IMRT treatment planning system. *J Appl Clin Med Phys 4*, 4 (2003), 341–51.

[51] MIAO, B., JERAJ, R., BAO, S., AND MACKIE, T. R. Adaptive anisotropic diffusion filtering of Monte Carlo dose distributions. *Phys Med Biol 48*, 17 (Sept. 2003), 2767–81.

[52] MORÉ, J. The Levenberg-Marquardt Algorithm: Implementation and Theory. *Numerical Analysis 630* (1978), 105.

[53] NELSON, W. R., HIRAYAMA, H., AND ROGERS, D. The EGS4 Code System. *SLAC-265, Stanford Linear Accelerator Center* (1985).

[54] NIYAZI, K. Quantitative Beschreibung des Phasenraums eines medizinischen Elektronen-Linearbeschleunigers durch Monte Carlo Simulation. Master's thesis, Eberhard-Karls-Universität Tübingen, 2008.

[55] PAELINCK, L., REYNAERT, N., THIERENS, H., DE NEVE, W., AND DE WAGTER, C. Experimental verification of lung dose with radiochromic film: comparison with Monte Carlo simulations and commercially available treatment planning systems. *Phys Med Biol 50*, 9 (May 2005), 2055–69.

[56] PATEL, I., GLENDINNING, A. G., AND KIRBY, M. C. Dosimetric characteristics of the elekta beam modulator. *Phys Med Biol 50*, 23 (Dec. 2005), 5479–92.

[57] ROGERS, D., WALTERS, B., AND KAWRAKOW, I. BEAMnrc users manual. Tech. Rep. PIRS-0509(A)revK, NRCC, Feb. 2007.

[58] ROGERS, D. W. Correcting for electron contamination at dose maximum in photon beams. *Med Phys 26*, 4 (Apr. 1999), 533–7.

[59] ROGERS, D. W., FADDEGON, B. A., DING, G. X., MA, C. M., WE, J., AND MACKIE, T. R. Beam: a monte carlo code to simulate radiotherapy treatment units. *Med Phys 22*, 5 (May 1995), 503–24.

[60] SALVAT, F., FERNANDEZ-VAREA, J. M., BARO, J., AND SEMPAU, J. PENELOPE, an algorithm and computer code for Monte Carlo simulation of electronphoton showers, 1992.

[61] SCHACH VON WITTENAU, A. E., COX, L. J., BERGSTROM, P. M., CHANDLER, W. P., HARTMANN SIANTAR, C. L., AND MOHAN, R. Correlated histogram representation of monte carlo derived medical accelerator photon-output phase space. *Med Phys 26*, 7 (July 1999), 1196–211.

[62] SEMPAU, J., WILDERMAN, S. J., AND BIELAJEW, A. F. DPM, a fast, accurate Monte Carlo code optimized for photon and electron radiotherapy treatment planning dose calculations. *Phys Med Biol 45*, 8 (Aug. 2000), 2263–91.

[63] SHEIKH-BAGHERI, D., AND ROGERS, D. W. O. Monte carlo calculation of nine megavoltage photon beam spectra using the beam code. *Med Phys 29*, 3 (Mar. 2002), 391–402.

[64] SHEIKH-BAGHERI, D., AND ROGERS, D. W. O. Sensitivity of megavoltage photon beam monte carlo simulations to electron beam and other parameters. *Med Phys 29*, 3 (Mar. 2002), 379–90.

[65] SIEBERS, J. V., KEALL, P. J., KIM, J. O., AND MOHAN, R. A method for photon beam monte carlo multileaf collimator particle transport. *Phys Med Biol 47*, 17 (Sept. 2002), 3225–49.

[66] SIKORA, M., AND ALBER, M. A virtual source model of electron contamination of a therapeutic photon beam. *Phys Med Biol 54*, 24 (Dec. 2009), 7329–44.

[67] SIKORA, M., DOHM, O., AND ALBER, M. A virtual photon source model of an Elekta linear accelerator with integrated mini MLC for Monte Carlo based IMRT dose calculation. *Phys Med Biol 52*, 15 (Aug. 2007), 4449–63.

[68] SIKORA, M., MUZIK, J., SÖHN, M., WEINMANN, M., AND ALBER, M. Monte carlo vs. pencil beam based optimization of stereotactic lung imrt. *Radiat Oncol 4* (2009), 64, doi: 10.1186/1748-717X-4-64.

[69] SJÖGREN, R., AND KARLSSON, M. Electron contamination in clinical high energy photon beams. *Med Phys 23*, 11 (Nov. 1996), 1873–81.

[70] SOLBERG, T. D., DEMARCO, J. J., HOLLY, F. E., SMATHERS, J. B., AND DESALLES, A. A. Monte Carlo treatment planning for stereotactic radiosurgery. *Radiother Oncol 49*, 1 (Oct. 1998), 73–84.

[71] SOLBERG, T. D., HOLLY, F. E., DE SALLES, A. A., WALLACE, R. E., AND SMATHERS, J. B. Implications of tissue heterogeneity for radiosurgery in head and neck tumors. *Int J Radiat Oncol Biol Phys 32*, 1 (Apr. 1995), 235–9.

[72] TILLIKAINEN, L., SILJAMÄKI, S., HELMINEN, H., ALAKUIJALA, J., AND PYYRY, J. Determination of parameters for a multiple-source model of megavoltage photon beams using optimization methods. *Physics in Medicine and Biology 52*, 5 (2007), 1441–1467.

[73] TSIAKALOS, M. F., THEODOROU, K., KAPPAS, C., ZEFKILI, S., AND ROSENWOLD, J.-C. Analysis of the penumbra enlargement in lung versus the quality index of photon beams: a methodology to check the dose calculation algorithm. *Med Phys 31*, 4 (Apr. 2004), 943–9.

[74] VAN BATTUM, L. J., VAN DER ZEE, W., AND HUIZENGA, H. Scattered radiation from applicators in clinical electron beams. *Phys Med Biol 48*, 15 (Aug. 2003), 2493–507.

[75] VAN ESCH, A., TILLIKAINEN, L., PYYKKONEN, J., TENHUNEN, M., HELMINEN, H., SILJAMÄKI, S., ALAKUIJALA, J., PAIUSCO, M., LORI, M., AND HUYSKENS, D. P. Testing of the analytical anisotropic algorithm for photon dose calculation. *Med Phys 33*, 11 (Nov. 2006), 4130–48.

[76] VENSELAAR, J., WELLEWEERD, H., AND MIJNHEER. Tolerances for the accuracy of photon beam dose calculations of treatment planning systems. *Radiother Oncol 60*, 2 (2001), 191–201.

[77] VERHAEGEN, F., AND SEUNTJENS, J. Monte Carlo modelling of external radiotherapy photon beams. *Physics in Medicine and Biology 48*, 21 (2003), R107–R164.

[78] WALTERS, B. R. B., AND ROGERS, D. W. O. DOSXYZnrc Users Manual. Tech. Rep. PIRS 794, NRC, 2004.

[79] WANG, L., CHUI, C. S., AND LOVELOCK, M. A patient-specific Monte Carlo dose-calculation method for photon beams. *Med Phys 25*, 6 (June 1998), 867–78.

[80] WANG, X., SPIROU, S., LOSASSO, T., STEIN, J., CHUI, C. S., AND MOHAN, B. Dosimetric verification of intensity-modulated fields. *Med Phys 23*, 3 (Mar. 1996), 317–27.